Licentiate of Philosophy Thesis
Medical Physics
Materials Research and Nanosciences

Feasibility Study of a Geant4-based Diagnostic X-ray Dose Simulator

Saana Jenu

May 4, 2019

Supervisors: Sauli Savolainen, Antti Kuronen, Mika Kortesniemi

Examiners: Jani Keyriläinen, Jarkko Ojala

University of Helsinki
Faculty of Science

HELSINGIN YLIOPISTO — HELSINGFORS UNIVERSITET — UNIVERSITY OF HELSINKI

Tiedekunta — Fakultet — Faculty	Koulutusohjelma — Utbildningsprogram — Degree programme
Matemaattis-luonnontieteellinen tiedekunta	Lääketieteellinen fysiikka Materials Research and Nanosciences

Tekijä — Författare — Author

Saana Jenu

Työn nimi — Arbetets titel — Title

Geant4-pohjainen annossimulaattori diagnostiseen röntgenkuvantamiseen

Työn laji — Arbetets art — Level	Aika — Datum — Month and year	Sivumäärä — Sidantal — Number of pages
Lisensiaatintyö	4.5.2019	60

Tiivistelmä — Referat — Abstract

Röntgenkuvaus on tärkeä diagnostinen menetelmä, jonka tuottaman sädeannoksen optimointi on oleellista terveyshaittojen ehkäisemiseksi. Monte Carlo -simulointia ei ole vielä käytetty laajasti röntgenkuvauksen optimointiin, mutta se on potentiaalinen menetelmä. Tämä työ on ensimmäinen askel HUS-Kuvantamisen ja Helsingin yliopiston käyttöön tarkoitetun Monte Carlo -annossimulaattorin kehittämisessä. Simulaattori toteutettiin Geant4-työkalulla, ja se perustui Geant4:n DICOM-ohjelmaan. Ohjelmaa kehitettiin edelleen, ja se testattiin yksittäisellä tietokoneella ja tietokoneklusterilla. Kehityksellä pyrittiin helpottamaan simulaattorin käyttöä ja mahdollistamaan suurten kuvapakkojen käyttö. Olennaisena osana työtä oli myös simulaattorin käytön dokumentointi sekä Monte Carlo -menetelmän kuvaaminen.

Työkalu lukee DICOM-muodossa olevat kuvat, minkä perusteella se muodostaa vokseleista koostuvan fantomin. Fantomin vokselit on luokiteltu eri materiaaleiksi HU-lukujen mukaan, jolloin hiukkasten kulkuratoja fantomissa voidaan laskea. Vokselit toimivat myös detektoreina, joihin absorboitunut energia tallennetaan.

Simulaattorin jatkokehityksen ja Monte Carlo -menetelmän kuvaamisen lisäksi simulaattoria testattiin keinotekoisilla ja tietokonetomografialaitteen tuottamilla DICOM-kuvilla. Sillä tehtiin kaksi testisimulointia, joissa arvioitiin intensiteettiä vedessä ja absorboitunutta annosta polymetyylimetakrylaatissa eri syvyyksillä. Tuloksia verrattiin teoreettisen intensiteetin vaimenemiseen ja MOSFET-antureilla mitattuun absorboituneeseen annokseen. Toinen simulaatio toistettiin kaupallisella ImpactMC-simulaattorilla.

Kahden simuloinnin tulokset poikkesivat referenssidatasta maksimissaan 5 % ja 17 %. Tarkempien tuloksien saamiseksi seuraavissa mittauksissa olisi hyvä käyttää herkempiä annosmittareita kuin nyt käytetyt MOSFET-anturit. Menetelmä, jonka avulla navigoidaan fantomin vokseleissa, on merkittävä sekä tulosten tarkkuuden että simulointinopeuden suhteen. Potentiaalisin menetelmä toimi kuitenkin huonosti klusterilla. Fantomin luomiseen tietokonetomografiakuvista saattaa vaikuttaa kuvien artefakta. Simulaattori vaatii vielä kehittämistä: jatkossa työkalun toimintavarmuutta ja laskentanopeutta klusterilla voidaan parantaa, ja työkaluun on mahdollista rakentaa geometriat eri röntgenmodaliteeteille.

Avainsanat — Nyckelord — Keywords

Dosimetria, Geant4, Monte Carlo, röntgenkuvantaminen, MOSFET

Säilytyspaikka — Förvaringsställe — Where deposited

Muita tietoja — Övriga uppgifter — Additional information

Surely I spoke of things I did not understand,
things too wonderful for me to know.

Job 42:3b

In the beginning you laid the foundations of the earth,
and the heavens are the work of your hands.

Ps. 102:25

Acknowledgements

I wrote this Licentiate Thesis as a part of my medical physicist qualification.

I am grateful to my supervisors Sauli Savolainen and Antti Kuronen for helping me to define the scope of the project and to keep it during the course of the work, and for their constructive comments, and to my supervisor Mika Kortesniemi for suggesting the original idea of simulation, for his valuable insights and help with measurements.

I am grateful to the examiners of this thesis, Jani Keyriläinen and Jarkko Ojala, for the review work and for helping me to improve the final version. Special thanks belong to Rebecca Craig and Ana Gheorghe for volunteering in proofreading the language in the thesis.

I thank Touko Kaasalainen, Teemu Mäkelä, Veli-Matti Sundell and Lauri Lehmonen for their help with measurements, and Hanna Halme for her tips with DICOM images. Many thanks belong to Eero Hippeläinen for his priceless advice and for explaining me the Monte Carlo method. I thank Camille Bélanger-Champagne for her help in using Geant4 on the cluster. I am grateful to Vesa Varjonen for supporting me in my medical physics studies during my work at Planmeca and Mari Varjonen for the chance to involve the work at Planmeca as a residency for the qualification. I thank Lasse Toimela for his tips with the code and Ismo Syrjä for his help with the computer.

I thank Geant4 Collaboration for providing the Geant4 toolbox and Louis Archambault, Luc Beaulieu, Vincent Hubert-Tremblay, Pedro Arce, Stephane Chauvie, Andrea Armando and Jonathan Madsen for sharing the simulator program DICOM. I am grateful to the Department of Physics at the University of Helsinki for allowing me to use their cluster, HUS Comprehensive Cancer Center and Planmeca for providing calculation computers and HUS Medical Imaging Center for permitting me to use their CT and MOSFET measurement equipment.

I want to thank my colleagues at HUS, North Karelia and Kymenlaakso Central Hospitals and Planmeca for teaching me medical physics in practice and for good company. I have learned so much from you!

I am grateful for the family for always supporting me in my studies and for my friends for all the encouraging words. Jeg ønsker å takke Jacob for all støtte og tålmodighet under det lange prosjektet.

Bergen, May 4, 2019

Saana Jenu

Nomenclature

CBCT	Cone-beam computed tomography
CERN	Conseil européen pour la recherche nucléaire (European Organization for Nuclear Research)
CLHEP	Computing library for high energy physics
CPU	Central processing unit
CSDA	Continuous slowing down approximation
CT	Computed tomography
CTDI	Computed tomography dose index
DCS	Differential cross section
DICOM	Digital imaging and communications in medicine
DLP	Dose-length product
GEANT	Geometry and tracking
GPU	Graphics processing unit
HU	Hounsfield unit
HVL	Half-value layer
IAEA	International Atomic Energy Agency
ICRU	International Commission on Radiation Units and Measurement
ImpactMC	Impact Monte Carlo
KERMA	Kinetic energy released per unit mass
keV	Kilo-electronvolt
LDPE	Low-density polyethylene
MC	Monte Carlo
MCNP	Monte Carlo N-Particle
MIRD	Medical internal radiation dose
MOSFET	Metal-oxide-semiconductor field-effect transistor
NIST	National Institute of Standards and Technologies
OpenDXMC	Open diagnostic X-ray Monte Carlo
OpenGL	Open Graphics Library
OSL	Optically stimulated luminescent
PCXMC	PC program for X-ray Monte Carlo
PDF	Probability distribution function
PMMA	Polymethyl methacrylate
PMP	Polymethylpentene
SLURM	Simple Linux for Resource Management
TLD	Thermoluminescent dosimeter
Voxel	Volumetric element

Contents

1. Introduction

X-ray imaging produces essential information about anatomy. However, the use of ionising radiation also increases the risk of cancer, genetic changes, or local tissue damage [1]. Therefore, optimisation of ionising radiation dose is necessary. Optimisation is especially important when a high radiation dose is used or a large number of people are exposed to radiation.

Computed tomography (CT) accounts for 58 % of the total radiation dose caused by X-ray imaging and interventional radiology in Finland, while the proportion of CT examinations is only 11 % [2, 3]. Recently, the number of CT examinations has increased [3, 4, 5]. This may be attributed to the improved CT performance, thanks to faster rotation times and a larger coverage. On the other hand, CT technology has developed several dose-saving methods. Correct application of these methods requires an exact understanding about dose distributions in the human body.

Interventional, conventional and dental radiology, as well as mammography can benefit from dose optimisation. In interventional radiology, patients are exposed to relatively high local radiation doses, and workers also receive a proportion of the dose. On the other hand, in conventional and dental X-ray examinations, a large number of people are exposed to ionising radiation, even though the radiation dose of an individual image is relatively low. Conventional radiology examinations account for 87 % of all radiological examinations in Finland [3], and the produced dose accounts for 12-16 % of the total dose exposure in Finland [2]. The number of cone-beam computed tomography (CBCT) examinations in dental radiology is increasing, and the dose in CBCT is much higher than that in traditional dental X-ray imaging. From 2011 to 2015, the number of CBCT examinations has increased nearly 9-fold [3]. Moreover, mammography could benefit from dose simulation, since breasts are highly radiosensitive organs regularly exposed to radiation dose in the course of screening programs [6].

In practice, dose optimisation requires methods to evaluate dose distribution and total dose in a patient. Radiation dose can be measured in the objects called phantoms. Measurement inside a human-mimicking, anthropomorphic phantom is performed by using small detectors such as thermoluminescent dosimeters (TLD), metal-oxide-semiconductor field-effect transistors (MOSFET) or optically stimulated luminescent (OSL) dosimeters. Using this method, point doses can be measured in a limited number of locations. Similarly, the dosimeter used by a radiation worker measures an approximation of radiation level by a point measurement. The dose descriptors reported by CT scanners, computed tomography dose index (CTDI) and dose-length product (DLP), are intended for comparing radiation out-

put from scanners, and they are not meant for the measurement of patient dose [7].

Computational dosimetry techniques are able to obtain dose distributions in any part of the human body, therefore providing more information than measurements. Dose in arbitrary tissues is important, since sensitivity to radiation and health risk vary among exposed organs [1]. The Monte Carlo (MC) simulation method is considered the gold standard for computational dosimetry [8]. In an MC simulation, X-ray photons are transported in the tissue by using information regarding interaction probabilities, and in some cases, secondary electrons are created. In this work, both a photon and an electron are referred to as a particle. Finally, the absorbed dose caused by the particles is calculated. MC simulations have already been used for a relatively long time in radiotherapy, but the large calculation capacity required has delayed the wider use of the method [9]. However, an available capacity is increasing [9], and many MC tools are also available for diagnostic radiology [10, 11, 12, 13, 14, 15, 16, 17, 18].

This work is the first step in introducing a dose simulator for the use of HUS Medical Imaging Center in Helsinki University Hospital. It is intended to be used at the computational cluster of the Department of Physics in the University of Helsinki. The simulator, created using the Geant4 (Geometry and tracking) toolbox [18], is based on the DICOM (Digital Imaging and Communications in Medicine) example [19] developed by the Geant4 users Louis Archambault, Luc Beaulieu and Vincent Hubert-Tremblay and reviewed and changed by Pedro Arce, Stephane Chauvie, Andrea Armando and Jonathan Madsen.

In this work, the goal is to assess how suitable the DICOM example program is in X-ray imaging. Suitability is assessed based on results and usability. Its usability is also improved by modifying the user interface. The theory of Monte Carlo simulation in X-ray imaging and the structure of the developed simulator are described in detail for the next developer of the tool. Finally, the simulator is tested with two simulations in simple geometries for calculation of absorbed radiation dose distribution. Further in the text, an absorbed radiation dose (Gy) is referred as an absorbed dose or a dose. In both simulations, the simulation geometries are built from a voxelised DICOM image. The first simulation models a monoenergetic pencil beam directed at a water-filled sphere and is compared with theoretical attenuation of intensity. In the second simulation, a diagnostic CT fan beam is modelled and directed at tissue-equivalent polymethyl methacrylate (PMMA). The simulated dose is compared with dose from MOSFET measurements. In addition, a simulation with a commercial simulator ImpactMC is used as a second reference [10]. The work also provides documentation of the simulator usage.

2. Monte Carlo method in X-ray imaging

2.1 Simulated physics

In X-ray imaging, an X-ray beam is directed at a patient, and the penetrated radiation is detected to form an image. Contrast between tissues is obtained through different attenuation properties. Attenuation is caused by photon scattering or photon energy deposition, when a photon interacts with the electrons of atoms.

X-ray interactions in tissue at the diagnostic energy range include Compton scattering, photoelectric effect and Rayleigh (coherent, classical) scattering. In Compton scattering, a fraction of energy is transferred to an electron, while the most of the energy is emitted further as a scattered photon. Compton scattering is major interaction in the soft tissue in X-ray energies, but its effect on local radiation dose is low. On the contrary, the photoelectric effect contributes to the local energy absorption through deposition of all photon energy to an electron. It predominates at low energies in the materials with a high atomic number. In Rayleigh scattering, an incident photon generates oscillation of electrons in the excited atom, and no energy is transferred to matter. It increases attenuation by a few percents, with its contribution being greater at low than high energies. [20, 21]

In diagnostic imaging, X-ray photons have a maximal energy in the range of 25-150 keV, while the mean energy is 50-70 % of the maximum. When a photon transfers its energy to an electron, the electron interacts repeatedly in the tissue by forming curved paths by reason of its electric charge. A 100 keV electron penetrates, on average, 0.14 mm from its departure point in liquid water [22]. Therefore, electrons are not often simulated in diagnostic X-ray energies. Instead, an approximation is generally made that energy is absorbed close to the point where it was deposited to an electron.

Radiation interaction is a stochastic process: it is impossible to predict the path of an individual X-ray photon, while a large number of photons behave in a deterministic way. However, the energy-dependent probability for different interactions of photons is utilised in MC simulations.

2.2 Monte Carlo concepts

The MC technique is a valuable tool in simulating X-ray interactions. It uses random numbers and random variables, which are quantities that cannot be predicted with

certainty and which are a result of repeatable processes [17]. A track of a particle, including that of a photon, can be understood as a random sequence of free paths and interactions that end as an energy loss and a creation of secondary particles. The interactions have different differential cross sections (DCS) that further define probability distribution functions (PDF) of the random variables.

When PDFs are known, they can be sampled with specific methods to create particle tracks. When a large number of tracks are calculated, these random processes can give information about deterministic processes such as formation of radiation dose. With a very large number of simulated particles, the MC method gives the same information about particle tracks as solving the Boltzmann transport equation. The Botzmann equation is complex to solve, while MC techniques are mathematically straightforward to implement. However, computing time in a MC simulation is long, and an insufficient time allowed for computation could result in a large statistical uncertainty.

A decision about the realization of an event occurs by sampling from the probability distribution. This is performed by using random numbers, or strictly speaking, by pseudorandom numbers. Pseudorandom numbers are created with algorithms, and they appear in random number sequences. In reality, they are not totally random but can be regenerated if the seed is known. Even though the goal is to have numbers that appear random, this reproducibility can be an advantage in scientific experiments. Pseudorandom numbers have two criteria: 1) every seed of a random number generator must lead to a unique number sequence. 2) a period of the sequence must be longer than the number of needed random numbers. [23]

2.3 Monte Carlo integration

Monte Carlo calculation can be presented as an integration. In the context of X-ray dosimetry, the radiation dose absorbed to a voxel is integrated over the total number of particles. Monte Carlo equations are applied here for dosimetry according to the presentation of the topic in [17]. Derivation is performed in one dimension, while the result is valid for many dimensions.

The integral

$$I = \int_a^b F(x)dx \tag{2.1}$$

defines the expectation value $\langle f \rangle$ of the dose:

$$I = \int f(x)p(x)dx \equiv \langle f \rangle, \tag{2.2}$$

where $F(x) = f(x)p(x)$, $f(x)$ is a simulated dose that was absorbed by one particle, and $p(x)$ is the PDF. $p(x) \geq 0$ in (a,b) and $p(x) = 0$ otherwise.

N random points x_i are generated from the PDF, and then the sum of the values $f(x_i)$ is calculated. The expected value of the absorbed dose for a limited number of particles is calculated as an average:

$$\bar{f} \equiv \frac{1}{N} \sum_{i=1}^{N} f(x_i). \tag{2.3}$$

When the number of simulated particles is very large, we can approximate for a finite and piecewise continuous $f(x)$

$$\bar{f} \to I. \tag{2.4}$$

Finally, the equation 2.3 can be written as

$$\langle f \rangle = \lim_{N\to\infty} \frac{1}{N} \sum_{i=1}^{N} f(x_i). \tag{2.5}$$

In this work, $\langle f \rangle$ is the average dose distribution, when N photons were used in the simulation. The absolute dose can be obtained with dose measurements in the same geometry.

2.4 Statistical uncertainty

As in any laboratory measurements, statistical uncertainty affects simulation results. The statistical uncertainty of the simulation is derived in this chapter according to [17], unless indicated otherwise. Variance is defined for the dose distribution $f(x)$ as [24]:

$$var(f(x)) \equiv \langle \{f(x) - \langle f(x) \rangle\}^2 \rangle. \tag{2.6}$$

By using the definition of an expectation value $\int f(x)p(x)dx$ like in equation 2.2, the variance becomes:

$$\langle \{f(x) - \langle f(x) \rangle\}^2 \rangle = \int (x - \langle x \rangle)^2 p(x) dx. \tag{2.7}$$

The PDF $p(x)$ has the following characteristics:

$$p(x) \geq 0 \tag{2.8}$$

$$\int_{x_{min}}^{x_{max}} p(x)dx = 1. \tag{2.9}$$

Therefore, the equation 2.7 can be rewritten as

$$var(f(x)) = \langle f^2(x) \rangle - \langle f(x) \rangle^2. \tag{2.10}$$

By applying the equation 2.5 for $f(x)$ and $f^2(x)$, we get :

$$var(f(x)) = \lim_{N\to\infty} \left\{ \frac{1}{N} \sum_{i=1}^{N} f^2(x_i) - \left[\frac{1}{N} \sum_{i=1}^{N} f(x_i) \right]^2 \right\}. \tag{2.11}$$

The equation 2.11 describes the variance of the dose distribution $f(x)$ calculated with the random numbers x_i for N photons. However, through the statistical nature of the Monte Carlo method, repetition of the simulation gives a different $f(x)$. To describe this statistical variation between dose distributions $f(x)$, $\bar{f}$ is termed an estimate of the dose distribution. $\bar{f}$ is a random variable with an unknown PDF. By

using properties of expectation and variance operators, the variance and the mean of $\bar{f}$ become

$$\langle \bar{f} \rangle = \left\langle \frac{1}{N} \sum_{i=1}^{N} f(x_i) \right\rangle = \frac{1}{N} \sum_{i=1}^{N} \langle f \rangle = \langle f \rangle \tag{2.12}$$

and

$$var(\bar{f}) = var\Big[\frac{1}{N} \sum_{i=1}^{N} f(x_i)\Big] = \frac{1}{N^2} \sum_{i=1}^{N} var(f(x)) = \frac{1}{N} var(f(x)). \tag{2.13}$$

The standard deviation of $\bar{f}$ is therefore

$$\sigma_f \equiv \sqrt{var(\bar{f})} = \sqrt{\frac{var(f(x))}{N}}, \tag{2.14}$$

where σ_f describes statistical uncertainty of the estimate $\bar{f}$ between separate simulations.

With $N \to \infty$, the PDF of $\bar{f}$ is a normal distribution with a mean $\langle \bar{f} \rangle$ and a standard deviation σ_f:

$$p(\bar{f}) = \frac{1}{\sigma_f \sqrt{2\pi}} \exp\left(- \frac{(\bar{f} - \langle f \rangle)^2}{2\sigma_f^2} \right). \tag{2.15}$$

Therefore, with a large N the uncertainty of simulation can be estimated with a practical equation

$$\sigma_f = \frac{1}{N} \sqrt{\sum_{i=1}^{N} f^2(x_i) - \frac{1}{N} \left(\sum_{i=1}^{N} f(x_i) \right)^2}. \tag{2.16}$$

The simulated dose is further multiplied with σ_f to obtain the final uncertainty. During the simulation, both $\sum_{i=1}^{N} f^2(x_i)$ and $\sum_{i=1}^{N} f(x_i)$ are saved separately for each voxel to use them in the calculation of the statistical uncertainty. The exact value $\langle f \rangle$ is in the interval $\bar{f} \pm n\sigma_f$ with a probability of 68.3 % when $n = 1$, 95.4 % when $n = 2$ and 99.7 % with $n = 3$. Generally, the uncertainty of 3σ is used in MC simulations.

The statistical uncertainty derived previously can be used to assess the necessary number of simulated particles. However, in some simulations, the method of simulating multiple independent batches of particles has been more convenient than the described method [25]. In the method using several batches, the final simulation result is calculated as a mean over the batches, and the statistical uncertainty as a standard deviation between the batches.

2.5 Monte Carlo simulation of radiation transport

This section is mainly based on the lecture material *Radiation effects of electron and photon radiation - biological materials* (A. Kuronen, personal communication

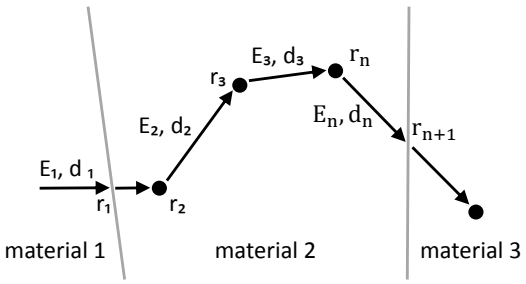

Figure 2.1: Radiation transport in three materials. The dots describe an interaction point and the lines boundaries between the materials. E, d and r are energy, direction and position in each state after interaction, respectively. Modified from *Radiation effects of electron and photon radiation - biological materials* (A. Kuronen, personal communication on October 18, 2018).

on October 18, 2018).

In MC simulation of radiation transport, particle paths are simulated step-by-step from one interaction to the next one (Fig. 2.1). After the interaction, the particle has a state described by its position $\bar{r} = (\bar{x}, \bar{y}, \bar{z})$, direction $\bar{d} = (\bar{u}, \bar{v}, \bar{w})$ and energy E. A series of states $(\bar{r_n}, \bar{d_n}, E_n)$ is called a track. The next state can be calculated by the following equations:

$$\bar{r}_{n+1} = \bar{r}_n + s\bar{d}_n \tag{2.17}$$

$$\bar{d}_{n+1} = R(\theta, \phi)\bar{d}_n \tag{2.18}$$

$$E_{n+1} = E_n - W, \tag{2.19}$$

where the free path length is

$$s = -\lambda_T \ln \xi. \tag{2.20}$$

R is a function of the angles θ and ϕ, and W is the deposited energy. ξ is a random number in $[0, 1)$. The average distance traveled by a particle between two interactions is called the total mean free path, and it consists of the mean free paths of possible interaction mechanisms, A and B:

$$\lambda_T = \frac{1}{\frac{1}{\lambda_A} + \frac{1}{\lambda_B}} = \frac{1}{n\sigma_T}. \tag{2.21}$$

The PDF of the path length is

$$p(s) = \frac{1}{\lambda_T} \exp(-\frac{s}{\lambda_T}). \tag{2.22}$$

The total cross section is the sum of the interaction cross sections:

$$\sigma_T(E) = \sigma_A(E) + \sigma_B(E). \tag{2.23}$$

Secondary particles are created in the interactions, and the simulation of the secondary particles is organised by pushing them to a stack. Paths of the secondary

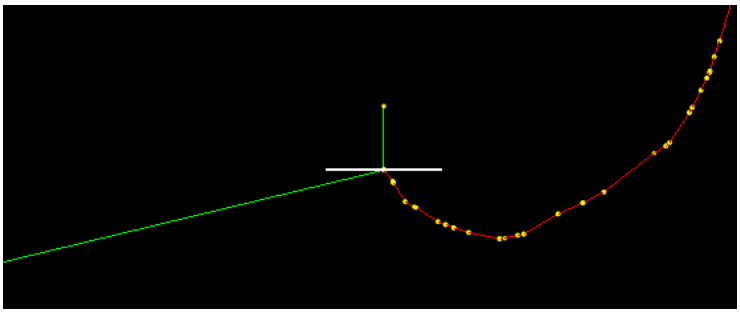

Figure 2.2: A 1-MeV photon directed at a 3 mm thick lead plate and the created photon and electron. The green describes photons paths, the red electron paths and the yellow interaction points.

particles are then simulated one by one until the stack is empty. Next, the transport of a new primary particle is started. Particles are simulated until their energy is below a defined threshold, and the energy is deposited locally. When the energy is deposited to the material, the coordinates and the mass of the voxel are saved to a file. Therefore, a voxel-wise absorbed dose (Gy=J/kg) can be calculated.

Photon attenuation is characterised by a mass attenuation coefficient, specific for material and energy. A photon does not have a mass and a charge, and therefore it has a long mean free path (Fig. 2.2). On the contrary, an electron interacts continuously with nearby molecules due to its electric charge, and its range is estimated with a continuous slowing down approximation (CSDA). It slows down in curved paths. Therefore, in order to accurately simulate electrons, a step length must be small.

2.6 Monte Carlo tools in diagnostic X-ray

MC simulation tools vary from readily available programs to general-purpose toolkits that can be used to create a user's own program. ImpactMC [9, 10], OpenDXMC (Open diagnostic X-ray Monte Carlo) [11] and PCXMC (PC program for X-ray Monte Carlo) [12] are examples of readily available medical X-ray simulation tools that do not require development from the user. ImpactMC models spiral CT, CT localizer, dual-energy CT, CBCT and radiography. Graphics processor units (GPU) and photon modelling without electron transport enable rapid calculation. A disadvantage with the tool is that the user cannot access or modify the code. An early version of a new tool OpenDXMC has been published recently. It has not yet been validated but is freely available. The tool is an open-source tool written with C and Python. The current version calculates dose for CT, and conventional radiographs have been planned. PCXMC targets on organ dose and effective dose calculation in conventional radiology and fluoroscopy. ImpactMC and OpenDXMC import DICOM images, while PCXMC uses only mathematical phantoms. None of these tools allow calculation of electron transport.

Examples of general-purpose particle tracking tools include Monte Carlo N-Particle Transport Code (MCNP) [13], Electron-Gamma Shower (EGS [14, 15] or EGSnrc [16, 26] from National Research Council of Canada), Penelope [17] and Geant4 [18]. They are versatile toolkits providing both photon and electron trans-

port in a large energy range. These tools provide the possibility to freely determine the geometry of the machine, spectrum, physics parameters and phantoms. However, they require in-depth understanding about the system and the code. Most of these codes use Fortran or a Fortran-based language, while Geant4 uses the C++ language.

2.7 Previous Monte Carlo simulation in diagnostic X-ray

MC techniques have been increasingly used in external radiotherapy dose calculation since the mid 1990s [27]. In X-ray imaging, the use of MC is now becoming more common due to the available computational capacity and awareness of radiation risks. Radiation dose in CT, conventional X-ray, interventional radiology, dental radiology and mammography has been simulated for research purposes. However, optimisation has not become a clinical routine, since many available MC tools are either complicated to use, or inflexible, or calculation is slow. In order to use MC tools, it is necessary to validate the used simulation geometry. Validation has often been performed with ionisation chamber, MOSFET, TLD or OSL measurements either in cylindrical or anthropomorphic phantoms, or against established data.

CT dose has been simulated in cylindrical PMMA phantoms [28, 29, 30], cylidrical water phantoms [31], mathematical phantoms [29, 32], anthropomorphic models created based on a CT image [30, 33, 34, 35, 36, 37, 38] or real patient CT data [32, 39, 40]. The aim has often been to estimate organ doses [29, 34, 39], and sometimes for a specific organ such as the lens of an eye [37]. The use of bismuth shielding is another example where Monte Carlo simulation proved to be useful [28]. Some studies have especially focussed on paediatric CT doses [34, 38, 39, 40] or dose of pregnant patients and foetus [29, 41]. Li et al published an extended study with full-body clinical CTs of 30 paediatric patients [39]. Ohno et al compared the dose of several multi-detector CT scanners [31]. In the study of Eeden et al, CT dose profiles and CT images were simulated [42].

X-ray doses in conventional radiography have also been simulated in cylindrical phantoms [8] and in anthropomorphic phantoms [25]. Dose exposure of patients with different weights, especially for obese patients, in radiographs was the focus in a study of Dedulle et al [8]. In another study, breast and lung dose in thorax radiography was investigated in both CT images and mathematical phantoms [43]. Effective doses of a patient and a radiologist in interventional radiology has been simulated in a rough medical internal radiation dose (MIRD) geometry by using MCNPX [44]. Siiskonen et al [44] investigated the effect of a lead apron in interventional radiology. Customisation of MC tools has also been implemented for CBCT [45, 46, 47]. MC proved to be a useful method for obtaining conversion coefficients for CBCT dose estimation, since standard CTDI measurements intended for CT are not suitable for large cones [47]. Mammography has recently been simulated to estimate X-ray spectrum in the breast [48] and to calculate mean glandular dose [6].

An energy spectrum for MC simulations has often been created with a separate X-ray modelling tool [29, 33] or with measurements [25, 42]. Generally used spectrum modelling tools include SpekCalc [49, 50, 51] and Spektr [46, 52]. Mam-

mography requires a spectrum created with a tool specific to mammography [48]. A spectrum can also be created with a simulation, but Monte Carlo simulation of electrons in an X-ray tube requires considerable computational power.

Electron transport is available in general-purpose systems and used by some studies [46]. In spectrum calculation, electron transport was naturally used [53]. However, many studies have chosen not to use electron transport due to long calculation times and a short electron range in diagnostic X-ray energies [6, 8, 29, 35, 42, 45] or it has not been available in the MC tool [30, 41, 43, 47]. In these cases, kinetic energy released per unit mass (KERMA) approximation has been used; local deposition of electron energy has been expected. In some studies, electron transport may have been simulated only in selected materials or objects [33].

Diagnostic imaging simulation has been performed with various tools: MCNP [28, 29, 32, 34, 35, 36, 37], EGS [8, 31, 42, 45, 46], Penelope [6, 33, 39, 40, 48, 53], ImpactMC [30, 41, 43, 47] and PCXMC [43]. Geant4 has not yet been widely used in diagnostic radiology, with the exception of a small number of studies [28, 38]. As a multi-purpose tool, Geant4 has been used in high energy simulations, nuclear and accelerator physics and space science. Its medical physics applications have been mostly photon and proton radiotherapy [54, 55], nuclear medicine, microdosimetry in cellular level and radiobiology [56]. In the current work, Geant4 was used, since it is a versatile tool using a modern programming language.

3. Geant4 in X-ray imaging

Geant4 is a MC toolkit simulating the interaction of particle beams in matter [18, 57, 58, 59]. It has been designed for particle physics simulations for the Large Hadron Collider in the European Organization for Nuclear Research (CERN), other high energy simulations and also for space and medicine applications. It includes electromagnetic, hadronic and optical processes with energies ranging from 250 eV to TeV energies in some cases. Passage of particles in matter is implemented with geometry, physics, processes, tracking and hits. The toolkit uses object-oriented programming, and functionality is defined in class categories and controlled by a run manager. Simulation requires certain data libraries according to the application. It is a user's task to define many of the classes in C++, while Geant4 offers examples to follow. However, creating a user's own simulator with the Geant4 toolkit necessitates certain requirements from the user, including understanding of particle physics, and C++ programming skills.

Geant4 software has been developed since 1994 by the Geant4 Collaboration which includes several institutions and individuals around the world. The source-code is freely available in internet [60], but it is limited by license conditions. Some parts of the toolkit are under a copyright owned by institutions and individuals. The Geant4 Collaboration does not give any warranty for the Geant4 software, nor does it have liability for its use.

3.1 Structure of the toolkit

The toolkit is organised in class-categories, which include geometry and materials, physics, tracking, hit management and event and track management. Geant4 is called a toolkit due to its modular structure, where a user can choose the components required for the application. Separate user action classes provide the user the possibility to customise Geant4 for a specific application. Development from a user is required to provide certain definitions such as a main function, geometry, materials, particles, physics processes and user actions. [18] The user compiles the code, which is then linked to Geant4's pre-compiled libraries [54].

Geometry is based on a geometrical object called *a solid*, which together with material information forms *a logical volume*. Materials are defined in the geometry class starting from the elements, their proportions and material densities. *A physical volume* is then created based on the logical volume and information about *a mother volume*, orientation and position. Complex solids can be created by using surface models. Detectors can then be assigned to volumes to allow particle detection. [18]

Particles are transported by the transportation process such that a particle

is either at rest, along step or post step. Particle transportation is organised in hierarchical levels which can be summarised as follows [54]:

- run: initialisation, termination and total control of particle histories,
- event: simulation of one history,
- track: a level between an event and a step, and
- step: advancing one step.

Each level in the list has its own manager classes, object classes, and may have user action classes.

Tracking is implemented separately from the transportation. This means that new physics processes could be added for a particle without the need to modify particle tracking. A tracking manager handles messages between objects used in transporting a particle. These objects are related for example to geometry and interactions. [18]

A step describes the minimum distance that a particle travels. At each step, particle information is updated: energy, position, direction, etc. A step size is selected according to the most limiting interaction process. The step size is an important factor regarding the reliability and efficiency of the simulation. [54] When the energy of an electron is discussed in this work, it refers to its kinetic energy.

3.2 Physical models

Physical models used in Geant4 are based on theory, experimental data and parameterisations [61]. Interactions of electrons, muons, positrons, photons, hadrons and ions are managed by packages of electromagnetic physics. The packages are divided into classes such as low energy and X-rays. In the electromagnetic package, the following processes are modelled: multiple scattering, ionisation, Bremsstrahlung, positron annihilation, photoelectric effect, Compton and Rayleigh scattering, pair production, synchrotron and transition radiation, Cherenkov effect, refraction, reflection, absorption, scintillation, fluorescence and Auger electron emission. A user can choose relevant physics processes for each particle type for the current application. [18]

Geant4 offers several electromagnetic packages with different physical models, i.e. the same process has multiple independent models. It is not clear, which electromagnetic package to use for diagnostic energies, and the choice is left up to the user. According to Amako et al [61], standard electromagnetic packages have been designed for energies between 1 keV and 100 TeV, while low energy packages are suitable down to 250 eV. The low energy packages include low-energy models for atomic and shell effects. [62] However, the Geant4 Collaboration recommends low energy models for applications of medical physics. For example the Penelope list, as a collection of physical models is called in Geant4, from the group of low energy physics packages is described to be suitable for any applications requiring higher accuracy of electron, hadron and ion tracking, when no magnetic field is modelled. [63] The Penelope list is adopted from the Penelope Monte Carlo Fortran code 2008 [17, 62]. Other low energy lists designed by Low Energy Electromagnetic Physics Working Group include G4EmLivermorePhysics (Livermore physics list)

and G4EmStandardPhysics_option4 (the most accurate models selected from the Standard and Low Energy lists) [64].

Geant4 always tracks particles until their kinetic energy reaches zero. Therefore, the amount of calculation can only be reduced by limiting the number of produced secondary particles. The number of secondary particles is controlled by setting production thresholds which are expressed as minimum distances travelled, and the distances are internally converted into energies in the particular material. When the set production threshold is higher than energy of the potential secondary particle, the energy is deposited locally. The threshold distance is 1 mm as default. [65, 66]

3.3 Validation in diagnostic X-ray energies

The Geant4 Collaboration has performed Geant4 validation in two levels. The obtained test results have been compared to databases, including the United States National Institute of Standards and Technologies (NIST) database and the International Commission on Radiation Units and Measurement (ICRU) database, and to publications. The first level includes microscopic quantities such as cross sections, angular and energy distributions, attenuation coefficients, stopping powers and CSDA ranges in different energies and materials. [61] Electromagnetic physics lists at the microscopic level, including the Penelope list, are in good agreement with the electromagnetic reference data from the NIST databases [62]. The second tested level concerns macroscopic quantities from complete detector set-ups. These simulations have been compared to experimental set-ups. It is considered important to verify the suitability of Geant4 models separately for each application. [61] Validation of complete diagnostic X-ray set-ups by the Geant4 Collaboration was not found in the literature, and therefore particular attention was paid to validation of the set-up used in this project.

Validation of Geant4 in medical physics by Carrier et al concerns radiotherapy energies [67]. However, particles were tracked down to keV energies, with production thresholds of 1-40 keV, which overlaps with diagnostic energies. Comparison with experimental data demonstrated less than 4 % difference. Moreover, there was no remarkable difference between Geant4 and other toolkits: MCNP, EGS4 and EGSnrc. [67]

4. Simulator

4.1 Structure

The simulator described in this work was used with Geant4 version 10.1, patches 1-3. User classes and import of DICOM images were taken from the example DICOM offered by Geant4 package 10.3 from 2016 (the folder `/examples/extended/medical/DICOM` in the package [19, 60]). The example was modified according to the needs of this simulation project. The general structure of the simulation is illustrated in Fig. 4.1. User action is required in the beginning with input files, when launching a simulation and at the end in visualisation. Input files include DICOM images, a CT calibration curve, tissue densities, a spectrum and other parameters, including geometry parameters. If the simulator is used in a computer cluster, a job scheduling file is also required. For example the Alcyone cluster [68, 69] in the Department of Physics at the University of Helsinki uses the Simple Linux for Resource Management (SLURM) [70] job scheduling tool for submitting a simulation.

After launching the program, DICOM images are converted into text files readable for Geant4, and a voxelised geometry is created based on the images. During runs, particles are transported and detected, and the absorbed dose is saved. As an output, the simulator gives text files including absorbed dose data (Gy), which a user can visualise for example with Matlab (MathWorks, MA, USA).

Detailed information about simulator development such as source files, modifications, known issues and further simulator development is available in Appendix A. User instructions are provided in Appendix B.

4.2 Geometry

Simulation geometry includes a photon source and a patient model inside a 4.0*4.0*4.0 m^3 cube filled with air. The photon source is implemented in a Geant4 macro file (App. B.2.3). The patient model is created based on the imported DICOM images. The simulator checks for possible overlapping volumes, because calculation may be inaccurate in overlapping volumes. For visualisation of geometry, the OpenGL tool can be used. Visualisation of a beam is recommended only with a small number of particles due to memory usage.

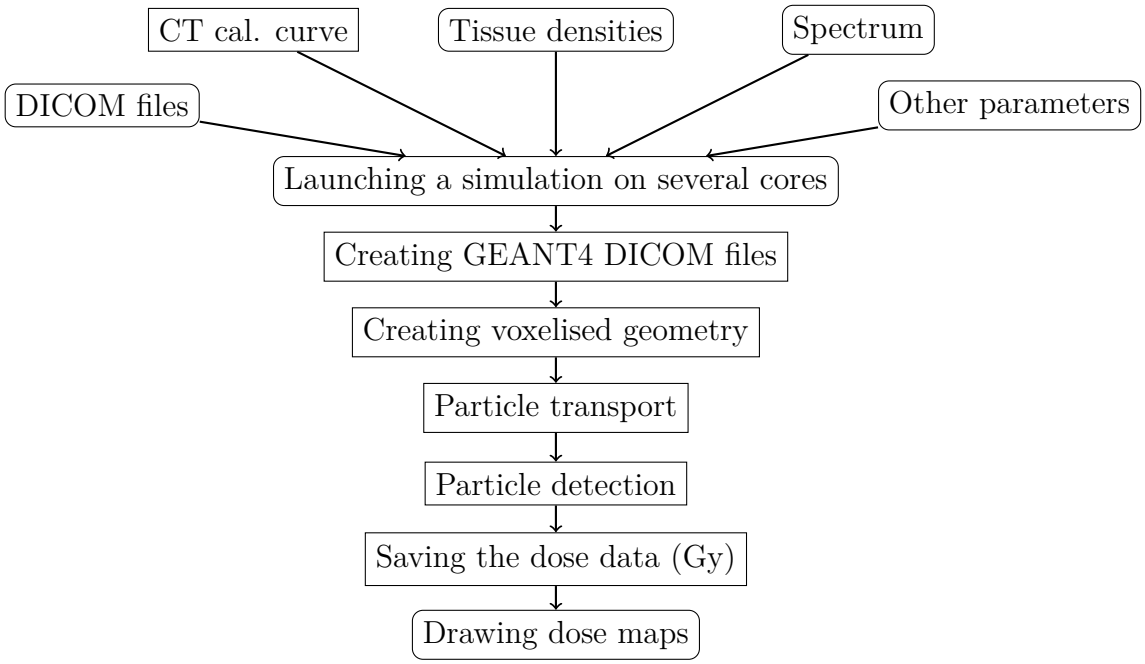

Figure 4.1: The structure of the simulator. Rectangles with rounded corners require user action. CT refers to computed tomography and DICOM to digital imaging and communications in medicine.

4.3 DICOM data

A patient model is imported to the simulator as CT slice images in the DICOM format. When launching the simulator, it first checks if Geant4 DICOM files have been created. If they are not found, they are created by making two conversions. First, Hounsfield unit (HU) information from the DICOM files is converted into densities (g/cm^3), and then the densities are classified as tissues. The classification is performed such that different types of tissue materials can be created, and each tissue is defined by density and proportion of chemical elements. Tissue classification could be used to define radiation dose in each tissue type, but that was not accomplished in this project.

By default, the HU-to-density conversion is performed based on the data from the Geant4 DICOM example [19] (Fig. 4.2, App. B.2.1) and the density-to-tissue conversion by using the tissue densities from ICRU [71] (Table 4.1, App. B.2.2). The HU-to-density conversion is different for each CT machine, and therefore users can replace the given conversion data with their own data. The density-to-tissue data from ICRU was referred through the reference from the Geant4 DICOM example [19]. An original DICOM slice and the corresponding image with classified tissues is shown in Fig. 4.3.

Data from the two conversions and other parameters are saved in the Geant4 DICOM files: in the decimal format in *.g4dcm* files, and the same in the binary format in *.g4dcmb* files. One file corresponds to one slice. The files contain information about material indices and densities for each voxel, and the exact form of the files is described in App. B.3. A user can choose if compression is done to hasten simulations by combining voxels of each slice to 2*2 voxels, 4*4 voxels, etc. Finally,

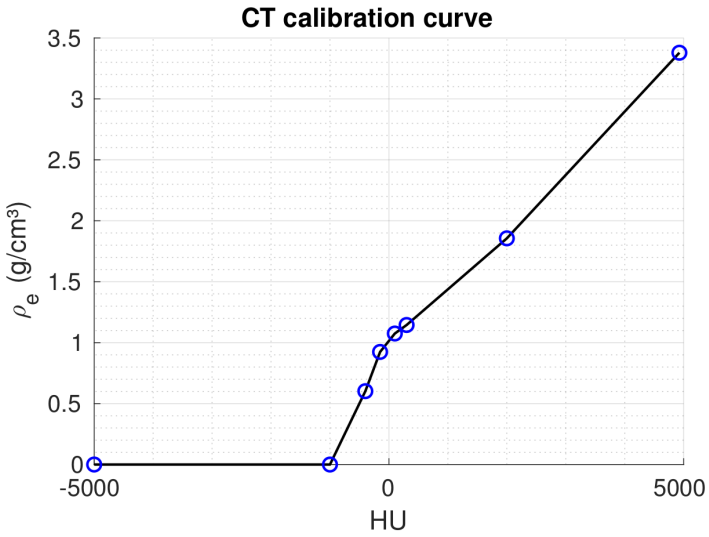

Figure 4.2: The computed tomography (CT) calibration curve from Hounsfield units (HU) to material density. The circles mark a data point, and the black line is an interpolation between them. [19]

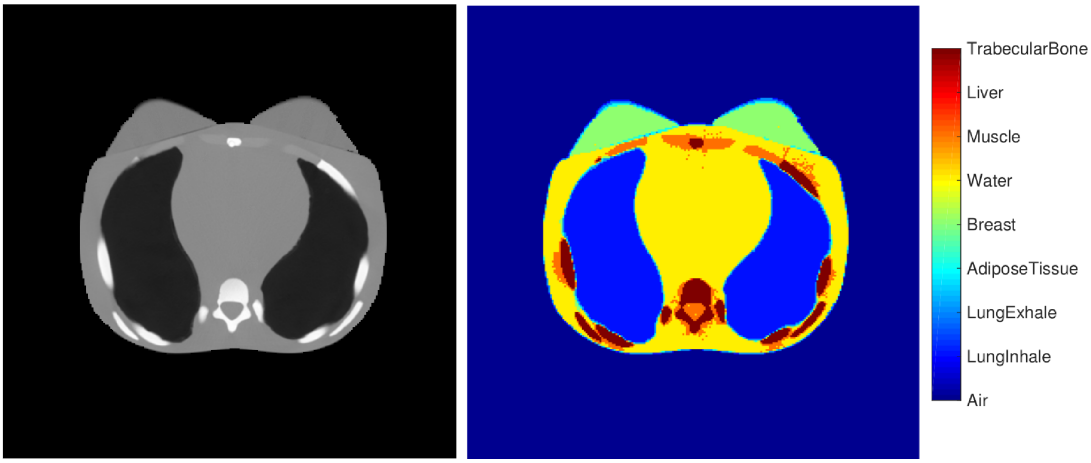

(a) An original CT image (DICOM). **(b)** Tissues classified in a Geant4 DICOM image.

Figure 4.3: Tissue classification in the Eunice phantom (adult female phantom model 702-D from CIRS, Norfolk, USA [72, 73]) imaged with a computed tomography (CT) scanner from General Electric with 120 kV. The voxelised model was created by using the calibration curve presented in Fig. 4.2. DICOM refers to digital imaging and communications in medicine.

Table 4.1: Density ranges for each tissue and material. [71]

Material or tissue	**Density (g/cm^3)**
Air	0.000-0.207
Lungs (inhale)	0.207-0.481
Lungs (exhale)	0.481-0.919
Adipose	0.919-0.979
Breast	0.979-1.004
Phantom	1.004-1.043
Liver	1.043-1.109
Muscle	1.109-1.113
Trabecular bone	1.113-1.496
Dense bone	1.496-1.654

information about tissues from all slices is merged to form a voxelised phantom which also works as a detector.

Segmentation of materials is a source of uncertainty in simulation, especially if CT images have artefacts. In addition, tissue composition may vary between individuals and inside one type of tissue.

4.4 Random number generator

The Mersenne Twister engine [74] is used in this simulator as a random number generator. The Mersenne Twister method was published in 1998 and adopted to Geant4 in 1998-2006. It is available in the Geant4 package (e.g. the folder `/geant4.10.01.p03/source/externals/clhep/src/MTwistEngine.cc` in the package). Mersenne Twister and many other random number engines are a part of Geant4's module Computing Library for High Energy Physics (CLHEP), and they inherit *HepRandomEngine*, which is an abstract class for random number engines [75].

For this work, Mersenne Twister was considered to be superior to older engines available in the Geant4 package such as *HepJamesRandom*, *DRand48Engine*, *MixMaxRng*, *RanluxEngine* and *RanecuEngine*. It is classified as a pseudorandom number generator with a very long period of $2^{19937} - 1$ numbers and accuracy of 32 bits, obtained with 624 words. It generates uniform random numbers in [0,1]. Matsumoto et al. [74] recommend Mersenne Twister for MC simulations.

The seed used in simulation is defined by the current Unix timestamp. The timestamp is the time at the moment of launching the simulator, including the year, month, day, hour, minute and second according to the system time. It is expected that only one simulator is started during the same second. The current version does not support a user's own seed, which can be used in the current version only by adding it in the code and by building a new software version.

4.5 Spectrum

The simulator does not create an energy spectrum for the X-ray beam, and it must be provided as an input file. Spectra can be modelled with an external program such as SpekCalc. SpekCalc was designed to be a research tool, and the tool does not provide any warranty for use. Therefore, one must be careful if it is used with calculations affecting patients as is the case with most MC tools. [76]

SpekCalc gives spectra based on EGSnrc MC data and theoretical cross sections. When developing SpekCalc, electron penetration, X-ray production and filtration were simulated in materials of high atomic number in energies of 50-150 keV, with a good agreement with measured data. [49, 50] Later the energy range was extended to 40-300 keV [77]. X-ray radiation created in an X-ray tube includes Bremsstrahlung radiation with a large energy spectrum and characteristic peaks. Bremsstrahlung radiation data was carefully created in SpekCalc, but characteristic peaks were calculated in a more approximate manner. That was considered adequate due to much smaller contribution of the characteristic radiation compared to Bremsstrahlung, which is valid for X-ray modalities except for mammography. [49, 50] SpekCalc is intended for anodes made of heavy elements similar to tungsten. Anodes used in mammography may be outside of this definition. However, rhenium (Z=75 and ρ =21.0 mg/cm^3), which is used in mammography, is essentially identical to tungsten (Z=74 and ρ =19.3 mg/cm^3). [49]

The user inputs the created energy spectrum to the simulator in a Geant4 macro file (App. B.7). The file consists of data pairs, each on a separate row. The first column defines an energy bin in MeV (as an upper edge for a bin), while the second column is weight. The first row is an exception: there is only one number that defines a lower edge of the first bin. The histogram can have a maximum of 1024 bins.

4.6 Dose calculation

Voxels of a volumetric patient model work as detectors and register the absorbed dose (Gy). Collecting the dose data requires navigation in the voxelised volume. Navigation has four options in the original DICOM program [19], which are available also for this simulator:

1. *Optimisation in a 3D grid with G4SmartVoxel*,
2. *1D optimisation*: after a track exits a voxel a decision about entering a new voxel is done in a loop over all other voxels,
3. *Nested parameterisation*: search of voxels is done hierarchically in 3D,
4. *Regular navigation (phantom parameterisation)*:
   A. Dose deposited to the last voxel of the material, and
   B. Dose deposited to each voxel.

The first option has a large memory usage but it is described to be fast, and the second option is certainly slow. The third option is fast and does not require much memory and could work in the simulation. [19]

The fourth option, regular navigation, can be used in two ways. Option 4A is the fastest option of all the available methods, since it deposits all energy to the last voxel of each material on the way of the photon track; borders inside one material are ignored. This method could work for an application where a total dose of each material is defined such as organ dose calculation. Nevertheless, an uneven distribution of dose might distort dose maps. The second regular navigation method (4B) calculates dose for each voxel. The dose that would have been deposited to the last voxel in method 4A is divided among the voxels on the way of the track. Division is done by taking into account the increase in energy loss per length and increase in multiple scattering while the particle decelerates. The method is iterative, and a two-step iteration was considered sufficient by the developers of the DICOM simulator. [19]

Regular navigation with fast calculation is the default method in the simulator. Instructions for configuring a method are described in App. B.2.5.

The simulator saves dose information in a text file (or several dose files). A Matlab script was created to draw dose maps equivalent to each DICOM image slice and to calculate attenuation.

5. Materials and methods

The simulator described in Ch. 4 is based on the Geant4 toolbox, the DICOM example provided by Geant4 and a few other Geant4 example codes. In this project, changes and additions to the DICOM program were performed to make the program suitable for the two tested geometries and to improve ease of use of the simulator. Details of the simulator development by the author of this work are given in App. A. The Geant4 toolbox has been previously validated (Ch. 3.3), but it was considered necessary to test the simulator in the current geometry. The aim of this work was to test the simulator in two simple geometries mimicking diagnostic X-ray imaging. Software testing outside the scope of the test simulations was not performed except for a simulation time test. A wider use of the simulator will require more development and testing. In addition to programming and testing, the author has provided detailed instructions regarding simulator set-up and its usage in the cluster (App. B).

The simulator was developed on a Hewlett-Packard Z600 computer with eight 2.67-GHz Intel Xeon central processing unit (CPU) cores in Ubuntu 16.04 with 7.8 GiB memory. Running the simulator in different environments was part of the feasibility testing of the simulator. Therefore, the usage of the simulator was tested both in Z600 and in the computing cluster Alcyone in the Department of Physics at the University of Helsinki. Alcyone is a cluster of 860 processor cores using Linux, and it is available for personnel and students of the university [68, 69]. Alcyone uses the SLURM batch job system to manage calculation [70]. The development of the simulator was performed outside the cluster. However, before the usage on Alcyone, the program was always built on Alcyone.

5.1 Simulation time

The choice of navigation method was based on accuracy, simulation time and usability. Since the regular navigation method (option 4A in Ch. 4.6) makes approximations that were visible in the preliminary simulations, other methods were preferred. Due to the approximations, dose distribution in a homogeneous material was not smooth. The second regular navigation method (4B) was not implemented in the code and was not available for simulation. 1D optimisation (option 2) was reported to be slow by the authors of the DICOM example program, and therefore it was not considered. Therefore, nested parameterisation (option 3) and 3D optimisation (option 1) were candidates for simulation. A short simulation time is essential in the practical use of a simulator. Therefore, simulation time per simulated particle per one CPU core was evaluated for the two methods. The list of physical models

used was EmStandard_opt4, and the voxel matrix was 256*256*101 pixels. Geometry consisted of a pile of PMMA plates, and the beam had a diagnostic spectrum as described in Ch. 5.3.2. The simulation time test was performed on the Z600 computer and the Alcyone cluster by simulating a known number of particles over two minutes. Cut ranges of secondary particles were also varied to understand its effect on the simulation time.

5.2 Attenuation of monoenergetic X-ray

Physical parameters of the simulation with a monoenergetic beam (simulation 1) are given in Table 5.1. Nested parameterisation was used as a voxel navigation method, and the simulation was performed on Z600. The reasons for the choice of the method and the computer are described in Ch. 6.1. The simulation was performed in parallel with eight CPU cores. The analysis of simulation data was performed with Matlab.

Table 5.1: Physical parameters in the Geant4 simulation of a monoenergetic pencil beam in a water-filled sphere (simulation 1) and of a diagnostic fan beam in polymethyl methacrylate plates (simulation 2).

Parameter	**Value**
Physics	Emstandard_opt4
Simulated particles	Photons, electrons
Simulated interactions	Compton scattering, photoelectric effect, gamma conversion, Rayleigh scattering, ionisation, Bremsstrahlung
Energy range cut, all particles (mm)	1.0 mm
Voxel navigation	Nested parameterisation

The simulation was executed in a simple geometry (Table 5.2), and the results were compared to theoretical attenuation of intensity. In the simulation, a monoenergetic photon pencil beam was directed to a water-filled sphere surrounded by air. The sphere model was a DICOM image created by using image processing. When creating a voxelised model of the sphere, the default HU-to-density calibration curve of the DICOM tool was used (Fig. 4.2). A beam energy of 70 keV was chosen as a mean energy of the diagnostic X-ray spectrum that will later be used in the second simulation (Ch. 5.3). Beam properties and cut ranges were configured by a Geant4 macro file shown in App. B.6.

Intensity, i.e. the number of traversing photons and electrons, was recorded in each voxel of the sphere and the surrounding air. Intensity included both photons and electrons, but the energy of electrons was approximated to be absorbed locally and to be constant over depth in the phantom. In practice, the intensity data were saved by collecting the number of particles instead of the deposited energy, and the change was made in the DicomRun.cc file (Table A.1). The simulation was performed in four independent batches of $6*10^8$ photons for evaluation of statistical uncertainty. Each batch therefore provided a 3D matrix, where voxel values represented the number of photons that have passed through that voxel. The overall

intensity of the simulation was calculated separately for each voxel as a mean over the batches and the statistical uncertainty as a 3σ deviation over the batches.

Theoretical attenuation serving as a reference was calculated according to the equation

$$\frac{N}{N_0} = e^{-(\mu/\rho)\rho x}, \tag{5.1}$$

where N_0 is in the number of incident photons, N the number of unattenuated photons, μ/ρ a mass attenuation coefficient in water, ρ density of water and x depth in water. This equation is valid for a monoenergetic, narrow X-ray beam. [21] The mass attenuation coefficient was interpolated between the coefficients of 60 keV and 80 keV to yield μ/ρ=0.1948 cm^2/g, and the density of water was 1.0 g/cm^3 [22].

Table 5.2: Parameters in the simulation of a water-filled sphere (simulation 1). DICOM refers to digital imaging and communications in medicine.

Parameter	**Value**
Original DICOM image size (px)	512*512
Compressed DICOM image size (px)	256*256
DICOM image size (mm)	380*380*160
Voxel size (mm)	1.5*1.5*2.5
Water density range in material classification (g/cm^3)	1.004-1.043
Water density in simulation (g/cm^3)	1.000 [22]
Water elements	H 11 %, O 89 % [22]
Air density in simulation (g/cm^3)	1.290 [22]
Air elements	N 70 %, O 30 % [22]
Centre of slices (mm)	(0,0,-190)
Position of the beam (mm)	(0.0,657.5,-190.0)
Direction of the beam	Down
Form of the beam	A pencil beam
Number of photons	4 batches of $6 * 10^8$
Seed number	20190206210510

5.3 Attenuation of diagnostic X-ray

The Geant4 simulation with diagnostic X-ray beam (simulation 2) used the same physical parameters as the simulation 1 (Table 5.1). It also made use of nested parameterisation, the Z600 computer parallel with eight CPU cores and Matlab for data analysis.

In simulation 2, a diagnostic CT beam was directed to a pile of PMMA plates. To simplify the geometry, the plate phantom was irradiated solely from one direction. The simulated absorbed dose was compared to the absorbed dose measured by MOSFET detectors in a similar geometry. One of the MOSFET measurements served as a calibration point for the dose level of the simulated dose. The MOSFET measurements served also as a reference for attenuation of the absorbed dose as a

function of the depth in PMMA. In addition, the ImpactMC simulator [10] was used as a second reference for the attenuation (simulation 3).

5.3.1 Measurements

For the calibration and the reference of the simulation 2, a pile of PMMA ($(C_5O_2H_8)_n$) plates was irradiated with a CT fan beam (Siemens Somatom Edge, Siemens Healthcare, Erlangen, Germany, Table 5.3). The absorbed dose was then measured at different depths with MOSFET detectors (Fig. 5.1a). Standard sensitivity MOSFET detectors from the Mobile MOSFET wireless dosimetry system (model TN-502RD, Best Medical, Canada [78]) were used in a high bias supply sensitivity. Calibration of the detectors was performed before the measurements with the same CT and the same X-ray spectrum (Fig. 5.1b). The MOSFETs were calibrated in air, while the measurements were executed in the PMMA.

Table 5.3: CT parameters and settings of Siemens Somatom Edge in the MOSFET measurement, which served as a reference to the simulation 2. The parameters were measured[1], from the scanner interface[2] or from personal communication with M. Kortesniemi on June 2018[3]. CT refers to computed tomography and MOSFET to a metal-oxide-semiconductor field-effect transistor.

Parameter	**Value**
Focus - plate surface distance (mm)	630 [1]
Focus - isocenter distance (mm)	595 [3]
X-ray tube voltage (kV)	120 [2]
X-ray tube current - time product (mAs)	200 [2]
X-ray direction	Down [2]
Slice collimation (mm)	64*0.60 [2]
Beam angle (°)	51 [3]
Focus	Small [2]
Bowtie filter	Body [3]

Dose was measured at five depths. The first measurement was performed closest to the surface, with MOSFET detectors being attached under PMMA plate 2 (Fig. 5.2). For practical reasons, one plate was added at a time to the top of the pile of plates, and the table was lowered by the same height (Table 5.4). Therefore, the distance between the focus and the surface of the pile was constant at all times. Plate 2 with holes for each detector was a calibration plate of the MOSFET system. Therefore, there was no air gap between the plates 1 and 2. The holes also ensured the correct orientation of the detectors. In each of the five measurements, all five MOSFET detectors were used (Fig. 5.3). The overall absorbed dose was calculated as an average over the five detectors at each depth. The 38.4 mm wide beam covered all five detectors with a margin of approximately 5 mm on each side. The variation in bowtie filter thickness in the area of detectors was estimated to be negligible, since the distances between the MOSFET detectors were small.

To choose suitable plates and to verify their materials to be PMMA, HU values of the plates were determined by imaging them with a CT (Siemens Somatom Definition Flash, Siemens Healthcare, Erlangen, Germany). Materials were esti-

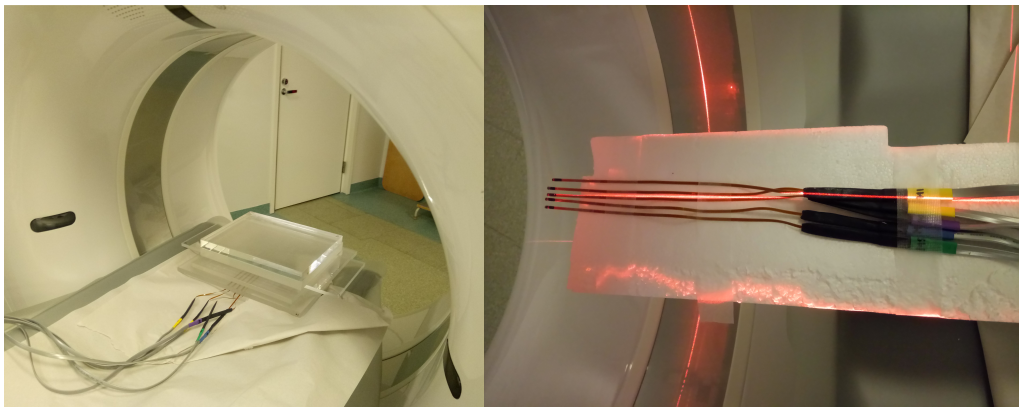

(a) MOSFETs in PMMA. **(b)** Air calibration of MOSFETs.

Figure 5.1: MOSFET measurement and calibration setups in CT. The MOSFET measurement served as a reference to the simulation 2. MOSFET refers to a metal-oxide-semiconductor field-effect transistor, CT to computed tomography and PMMA to polymethyl methacrylate.

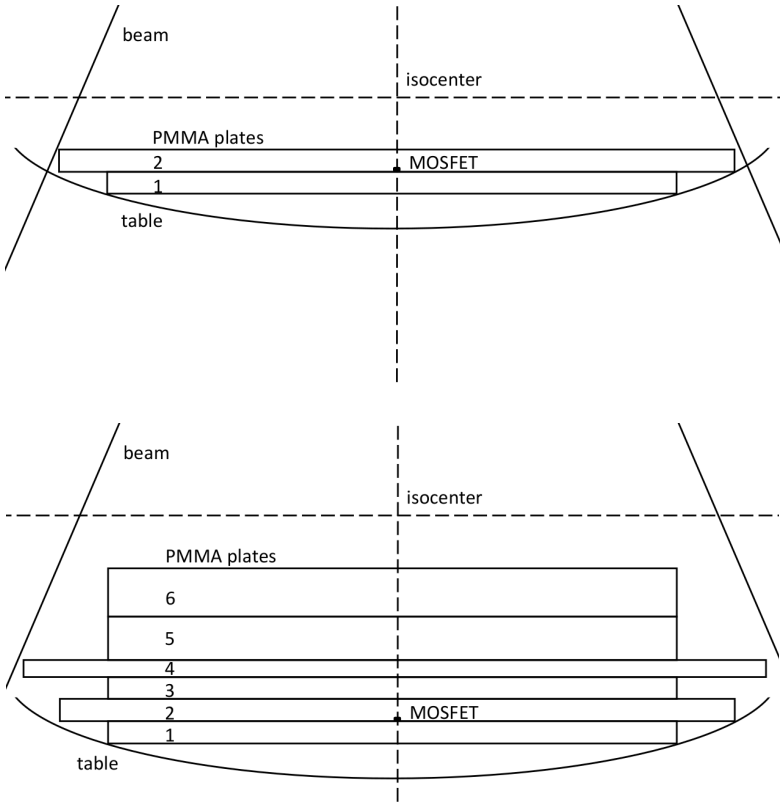

Figure 5.2: Polymethyl methacrylate (PMMA) plates in the first (top) and the last (bottom) MOSFET measurement. MOSFET refers to a metal-oxide-semiconductor field-effect transistor.

Table 5.4: Characteristics of the polymethyl methacrylate (PMMA) plates in the MOSFET measurements for the second simulation. HU refers to Hounsfield unit and MOSFET to a metal-oxide-semiconductor field-effect transistor.

Measurement	**1**	**2**	**3**	**4**	**5**
Added plates	1 & 2	3	4	5	6
HU value of the added plate	125 & 125	132	132	130	133
Thickness of the added plate (mm)	10 & 10	10	8	19	21
Depth of MOSFET detector (mm)	10	20	28	47	68
MOSFET - isocenter distance (mm)	35	45	53	72	93
Table height, increasing ↓ (cm)	100	110	118	137	158

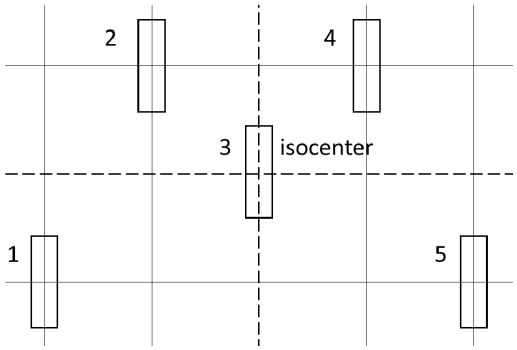

Figure 5.3: Metal-oxide-semiconductor field-effect transistor (MOSFET) detectors in the holes under the polymethyl methacrylate (PMMA) plate 2. The grid size in the image is 1.0 cm * 1.0 cm.

mated from regions of interest from axial slices, and the HU values of the plates were compared to that of the calibration plate (plate 2) which was known to be PMMA (Table 5.4). Small variation between the HU values of the chosen plates was considered negligible.

The chosen plates had different sizes, the smallest plate in the lateral direction being 25 cm, and the smallest in the longitudinal direction being 15.5 cm. In the lateral sides, the X-ray beam reached more than 24-27 cm from the MOSFET detectors, depending on the position of the detectors. Hence, the size of the beam and the plates in lateral direction were considered to be sufficiently large such that small variation in them would not affect scatter near the detectors. In the longitudinal direction, the beam was 38.4 mm wide, and the plates were considered large enough such that different plate sizes did not affect the amount of scattering in the MOSFETs.

The uncertainty of the measurements was affected by several characteristics of the MOSFETs such as bias supply sensitivity, energy dependence and angular dependence. Bias supply sensitivity of 20 cGy doses is $< 3\%$ for the used MOSFETs [78]. Doses used in the measurement were lower than 20 cGy, approximately 1.5-4 cGy, and therefore bias supply sensitivity was possibly higher than 3 %. Energy dependence of the MOSFET detectors was taken into account by using the same X-ray spectrum for MOSFET calibration and measurements. Small deviation from the original spectrum may have been present due to X-ray beam hardening in the

PMMA. However, the effect of beam hardening was considered to be negligible, as the thickest amount of PMMA between the focus and a MOSFET was 68 mm. The angular dependence of 5 %, 8 % and 7 % in the equivalent MOSFET detectors (model TN-1002RD-H, Best Medical, Canada) has been measured in axial, normal-to-axial and tangent-to-axial rotations in PMMA, respectively [79]. In our set-up, primary radiation reached MOSFETs from one direction in their sensitive side, but angular dependence may have affected the measured scattered radiation. Positioning of the detectors and vertical movement of the table between the experiments are potential sources of uncertainty but can be considered small.

The sum of the uncertainties from the described MOSFET characteristics and positioning of the MOSFETs was estimated based on the standard deviation of the calibration measurements. Scattering conditions were different in the calibration in air and in the actual measurements in PMMA. Air calibration was performed by repeating five measurements for each of the five MOSFETs, and the uncertainty of one MOSFET was defined as an average 3σ deviation of the five measurements. Based on the variance of a sum [24]

$$\sigma_{X+Y}^2 = \sigma_X^2 + \sigma_Y^2, \tag{5.2}$$

the uncertainty of a MOSFET measurement was calculated from five air calibration uncertainties σ_i:

$$\sigma = \sqrt{\frac{\sum_{i=1}^{5} \sigma_i^2}{5}}. \tag{5.3}$$

5.3.2 Simulations

The simulations 2 (Geant4) and 3 (ImpactMC [10]) mimicked the reference measurements (Ch. 5.3.1). This chapter describes in detail the performance of the Geant4 simulation. ImpactMC simulation was carried out in the similar geometry, but the details of the software can be studied elsewhere [10].

In the simulation 2, a voxelised model was created by imaging the PMMA plates used in the MOSFET measurements with Siemens Somatom Edge (Table 5.5). Equivalent geometry could have been programmed directly to Geant4, but the goal of validation was to test the whole chain of the simulator, including the import of DICOM images (Fig. 4.1). The plates were imaged in a similar pile as in the last MOSFET measurement (Fig. 5.2 and Table 5.4). Technically, the order of the plates in the CT image was not the same as in all MOSFET measurements, since the topmost plate in the pile changed for each measurement. That should not affect attenuation, since the HU value variation among the plates was small and no air gaps were left between the plates. The patient table was also modelled, even though it does not have influence on the simulated absorbed dose, since the beam does not enter PMMA through the table. In the simulation 3, a similar CT image was used, even though for practical reasons the image was from a different imaging session.

When creating the voxelised model, the DICOM program requires a calibration curve to determine material densities (g/cm^3) from HU values. Therefore, the calibration curve was measured with Siemens Somatom Edge by using the CTP404

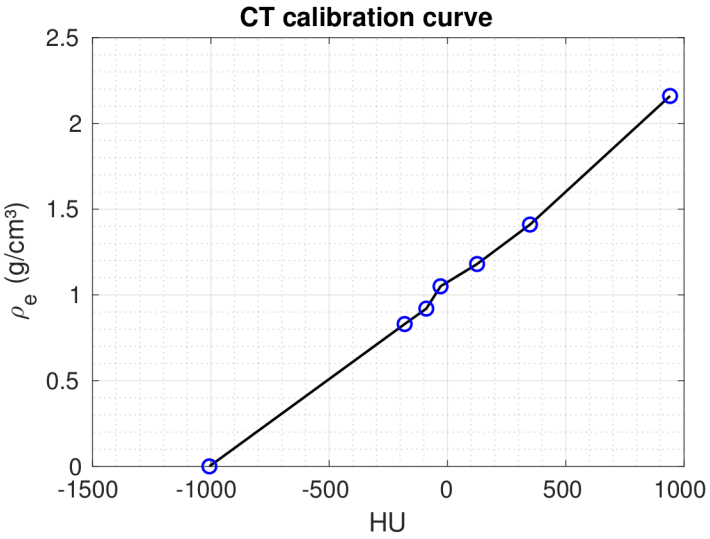

Figure 5.4: The computed tomography (CT) calibration curve from HU to material density measured using Siemens Somatom Edge and the Catphan 600 phantom. The circles mark data points, and the black line is an interpolation between them. The measured data points included in the increasing order of density: air, polymethylpentene (PMP), low-density polyethylene (LDPE), polystyrene, acrylic, Delrin and Teflon. HU refers to Hounsfield unit.

module of the Catphan 600 phantom (The Phantom Laboratory Inc., Salem, NY, USA). The imaging protocol of the voxelised phantom described previously was used to ensure the same spectrum and image reconstruction, and therefore comparable HU values (Table 5.5, Fig. 5.4).

Table 5.5: Computed tomography (CT) protocol in Siemens Somatom Edge used for measurements of HU-to-density calibration curve and for imaging of polymethyl methacrylate (PMMA) plates to create a voxelised phantom. HU refers to Hounsfield unit.

Parameter	**Value**
Protocol	Abdomen native
X-ray peak energy (keV)	120
Eff. tube current - time product (mAs)	400
Kernel	B30f medium smooth

Simulation geometry parameters of the simulation 2 were chosen according to the measurement geometry, and they were verified with the OpenGL visualisation. The DICOM images of the PMMA plate were converted into a voxelised model by using the measured HU-to-density calibration curve and the parameters shown in Table 5.6. The images were compressed from 512*512 pixels to 256*256 pixels. The simulator places image data according to scanner coordinates: the PMMA plates were not centered exactly in the z-direction in the scanner, and therefore the z-coordinate was not zero. The PMMA and air of the voxelised model were in a 4.0 m*4.0 m*4.0 m cube of air.

In the simulation 2, the plate model was irradiated from above with a circular-shaped cone-beam collimated with two 3 mm thick lead plates in the z-direction (Fig. 5.5). This was done to produce a similar amount of scatter from PMMA as in

Table 5.6: Parameters and values in the Geant4 simulation (simulation 2) with polymethyl methacrylate (PMMA) plates. DICOM refers to digital imaging and communications in medicine.

Parameter	**Value**
Original DICOM image size (px)	512*512
Compressed DICOM image size (px)	256*256
DICOM image volume (mm)	394*394*210
Voxel size (mm)	1.5*1.5*1.0
PMMA density range in material classification (g/cm^3)	1.00-1.19
PMMA density in simulation (g/cm^3)	1.19 [22]
Elemental composition of PMMA	H 8 %, C 60 %, O 32 % [22]
Air density in simulation (g/cm^3)	1.29 [22]
Elemental composition of air	N 70 %, O 30 % [22]
Centre of slices (mm)	(0,0,408)
Position of the focus	(0,633,408)
Direction of the beam	Down
Shape of the beam	A circular-shaped 51° cone collimated from cranial and caudal sides
Collimator material	Pb
Collimator sizes (mm)	(300,3,200)
Collimator positions (mm)	(0.0,481.0,303.5/512.5)
Number of photons	10 batches of $2 * 10^9$
Seed number	20190210120651

the MOSFET measurement and because the Geant4 code does not include a macro command for a fan beam. The lead plates were at the distance of 152 mm under the focus, and the slit between the lead plates was 10.0 mm wide, which resulted in a beam width of approximately 40 mm at the isocenter. The beam width of 40 mm corresponded to the collimation 64*0.6 mm used in the MOSFET measurements (Table 5.3). The simulated focus of the X-ray beam was a point source, which is not the case with a physical X-ray tube. However, the difference in the focus size was considered small for the present dose simulation. In summary, the geometry parameters focus - plate surface distance, collimation and beam angle were carefully chosen according to the parameters of the physical scanner, while the focus size and bowtie filter were not modelled.

The spectrum of the simulations 2 and 3 was created with SpekCalc [76] with the parameters shown in Table 5.7 (Fig. 5.6). The aim was to create a similar spectrum to that of Siemens Somatom Edge in the MOSFET measurement. According to Siemens, a typical half-value layer (HVL) for a spectrum with a peak energy of 120 keV is 8.4 mm of aluminium [80]. That HVL was used to define the thickness of aluminium used as a filter, i.e. 11.35 mm, with SpekCalc. The bowtie filter of the CT was estimated to be approximately flat in the centre, i.e. at the locations of MOSFET detectors. The simulated CT has an anode at an angle of 7°, coating made of a tungsten-rhenium solution [80]. Simulation of a spectrum with SpekCalc

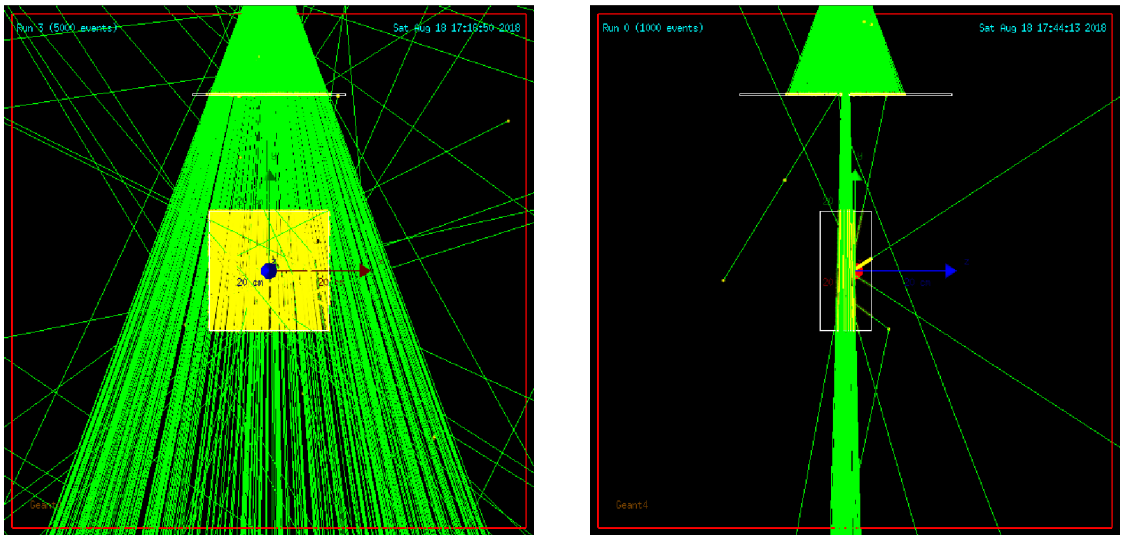

Figure 5.5: Visualisation of the Geant4-simulated beam in the simulation 2 towards the negative z-axis with 3000 X-ray photons (left) and towards the positive x-axis with 300 photons. The green colour marks photon tracks and the yellow interaction points. The box in the centre is the voxelised model, and the collimators are visible on top of the images. The scales show 20 cm: red in the x-axis, green in the y-axis and blue in the z-axis. The size of the boxes is 80 cm * 80 cm.

applies to this type of anode [49]. An output normalisation factor Nf can be used to match calculated and measured outputs (μGy/mAs), but it was kept at its default value, since only the form of the spectrum was important. The normalisation factor P for characteristic radiation to Bremsstrahlung radiation, was also kept at its default value. In addition to the HVL and to the anode angle, no other information was available about the X-ray tube of the scanner. The energy spectrum and the intensity of the X-ray beam were expected to be constant in every beam angle.

Table 5.7: SpekCalc parameters and values used in the creation of the diagnostic fan beam for the simualtions 2 and 3 (Geant4 and ImpactMC).

Parameter	**Value**
X-ray peak energy (keV)	120
X-ray minimum energy (keV)	12.5
X-ray energy bin (keV)	0.5
Anode angle (°)	7
Air thickness (mm)	1000.00
Aluminium thickness (mm)	11.35
Nf, the output normalisation factor	0.68
P, the normalisation factor	0.33

The number of photons used in the simulation 2 was $2 * 10^{10}$. The statistical uncertainty analysis for the simulation was performed in two ways, using the equation 2.16 and calculating the mean and the standard deviation over 10 batches of $2 * 10^9$ photons. For the first statistical uncertainty analysis, the term $\langle f^2 \rangle$ was obtained by repeating the same simulation as that for $\langle f \rangle$ with the same seed but collecting the squared dose data instead of dose data. The reported statistical un-

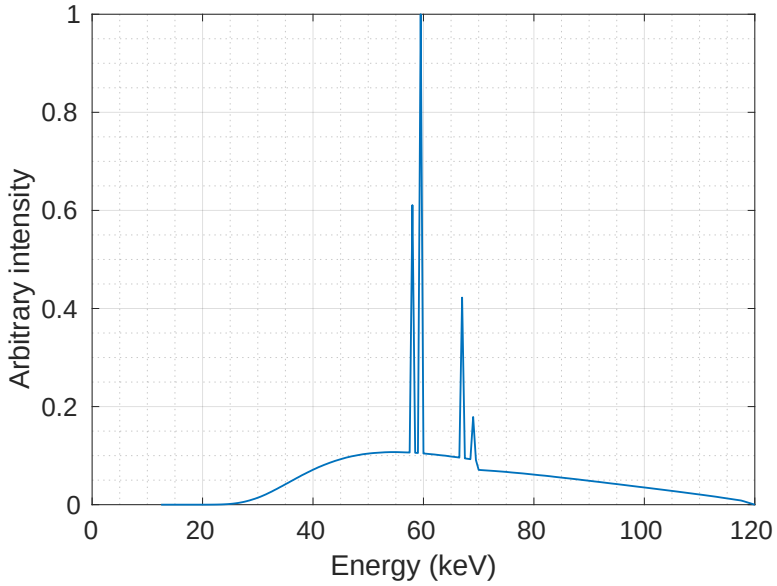

Figure 5.6: The X-ray energy spectrum with a peak energy of 120 keV used in the simulations 2 and 3 (Geant4 and ImpactMC). The spectrum was created with SpekCalc, and it mimicks diagnostic X-ray energies.

certainty was defined as a 3σ deviation. The macro file used for the simulation is shown in App. B.7.

6. Results

6.1 Simulation time

The results of the computation time test with Geant4 are shown in Table 6.1. The test results show that the 3D optimisation method (option 1) was slow; the simulation time being 548 times longer than that with the nested parameterisation and 472 times longer than that with the regular method. Simulation time per CPU core was approximately the same on Alcyone and Z600. Cut ranges had small differences, and any of the three cut ranges was considered usable in the simulations.

The nested parameterisation method (option 3, Ch. 4.6) did not work properly on Alcyone leading to a "segmentation fault" during the run, although it mostly worked on Z600 with the same settings. Nested parameterisation sometimes failed to launch the simulator in Z600, but the problem could be bypassed with a reboot of the program. To evaluate the speed of computation on Alcyone, the regular navigation method (option 4A) was tested even though it was not used in the final simulations.

Table 6.1: Simulation times/central processing unit core in the geometry of polymethyl methacrylate (PMMA) plates with Geant4. In the navigation column, 3D opt refers to optimisation in a 3D grid (option 1, Ch. 4.6), nested to nested parameterisation (option 3) and regular to regular navigation (option 4A).

Computer	**Navigation**	**Cut range**	**Time/ photon**
Z600	Nested	1 mm	0.062 ms
Z600	Nested	10.0 mm	0.066 ms
Z600	Nested	0.1 mm	0.066 ms
Z600	3D opt	1.0 mm	34.000 ms
Z600	Regular	1.0 mm	0.072 ms
Alcyone	Regular	1.0 mm	0.069 ms

6.2 Attenuation of monoenergetic X-ray

In the simulation 1, the voxel model of a water-filled sphere was formed from the DICOM image created with image processing (Fig. 6.1a). Tissue classification was performed as described in Ch. 4.3 (Fig. 6.1b). Computational time for $2.4*10^9$ photons with the DICOM simulator was 49.2 h with the 8 CPU cores of Z600. The

simulation was performed in four batches of $6*10^8$ photons, and a visualisation of one batch is shown in Fig. 6.1c. The two voxels wide central column visible in the image with higher intensity than its surroundings was used in the attenuation calculations. Attenuation was calculated as an average of intensities in the four batches and the statistical uncertainty as a 3σ deviation between the intensities in the four batches (Fig. 6.2). The calculated statistical uncertainty in the Geant4 simulation was small. Since the goal was not to investigate boundary effects in the interface between air and water, plotting of intensity was started at a depth of 3 mm from the surface of the water-filled sphere. The theoretical and simulated intensity curves were normalised at the maximum, where intensity was set to 1. The start and the end of the intensity data are additionally shown in Fig. 6.3 and 6.4 for a detailed inspection. The difference of the simulated intensity compared to the mass attenuation data of NIST [22] was less than 5 % (Fig. 6.5).

6.3 Attenuation of diagnostic X-ray

The CT image used for the simulations 2 and 3 is shown in Fig. 6.6a. This image and the entire image data set in the DICOM format was succesfully imported to the simulator. Variation in HU values is visible resulting from the air between the plates and in the uppermost plate due to CT artefact. PMMA and air were classified from the CT image along with other materials and tissues (Fig. 6.6b), and the variation of the HU values can also be seen in that image, where a proportion of the PMMA is classified as muscle and other tissues. The structures below the plates are a table and a mattress that are part of the CT scanner. The third image (Fig. 6.6c) shows the simulated absorbed dose in air, in the plates and in the CT structures. The three images are shown in the centre of the fan beam such that the image plane is perpendicular to the longitudinal axis of the table. Computational time for $2*10^{10}$ photons with the DICOM simulator was 68.3 h with the 8 CPU cores of Z600.

The measured and simulated absorbed dose in PMMA as a function of depth are shown in Fig. 6.7. At each depth from the surface of the plates, simulated absorbed dose was calculated as an average over 6 mm in the lateral direction and 4 mm in the longitudinal direction to reduce noise. That was done in the same way for the Geant4 and ImpactMC data. The MOSFET holes visible in the centre slice where not in the analysed region (Fig. 6.6). The statistical uncertainty of the simulation was first evaluated according to Eq. 2.16. However, the statistical uncertainty was minimal even where large variation was visible in the data. Therefore, to have a practical means for defining error bars, the statistical uncertainty was calculated as a 3σ deviation from 10 independent batches of $2*10^9$ photons, similarly to Ch. 6.2.

Geant4 simulation gave a relative dose distribution, and therefore the Geant4-simulated absorbed dose was normalised to the MOSFET measurements. Normalisation was performed based on the second MOSFET measurement at a depth of 20 mm. The second measurement point was chosen for normalisation, because it minimised the sum of the differences between the Geant4 simulation and the MOSFET measurements. MOSFET detectors measure air KERMA (kinetic energy released per unit mass), since they were calibrated against CT ionisation chamber measure-

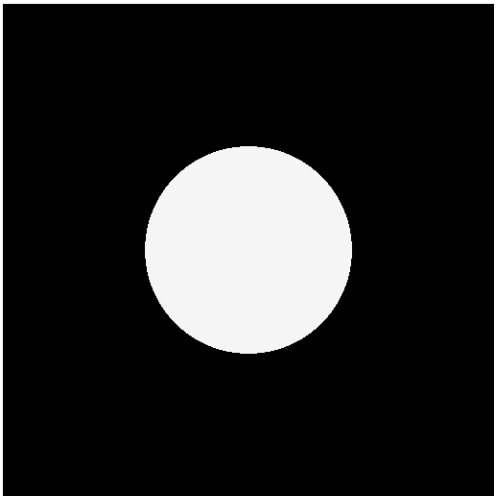

(a) The DICOM image created with image processing for the simulation in water. The HU value of the water-filled sphere is 0, and that of air in the background is -1000.

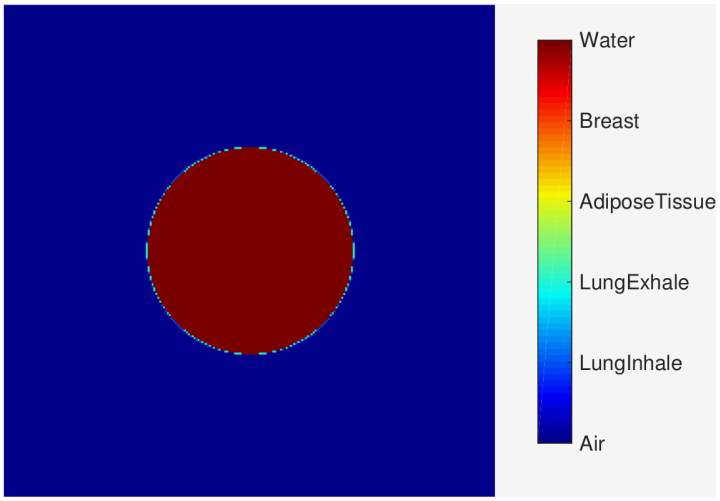

(b) Classification of materials and tissues of Fig. 6.1a performed with the DICOM program.

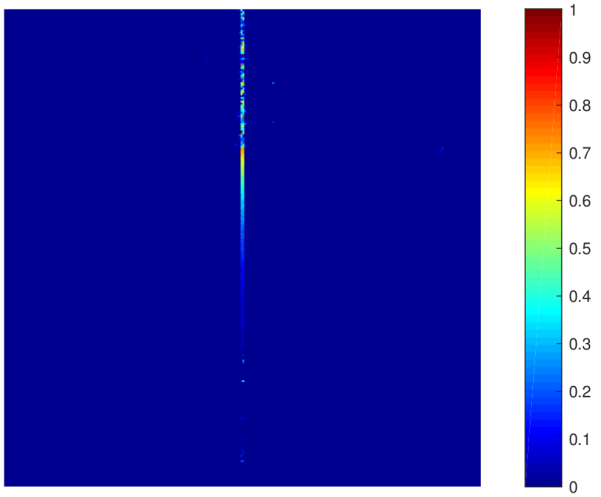

(c) Voxel-wise particle intensity in the water-filled sphere and in air simulated with the DICOM program by using the materials and tissues of the Fig. 6.1b (arbitrary units).

Figure 6.1: The centre slice of the water-filled sphere image in air used in the simulation 1. DICOM refers to digital imaging and communications in medicine.

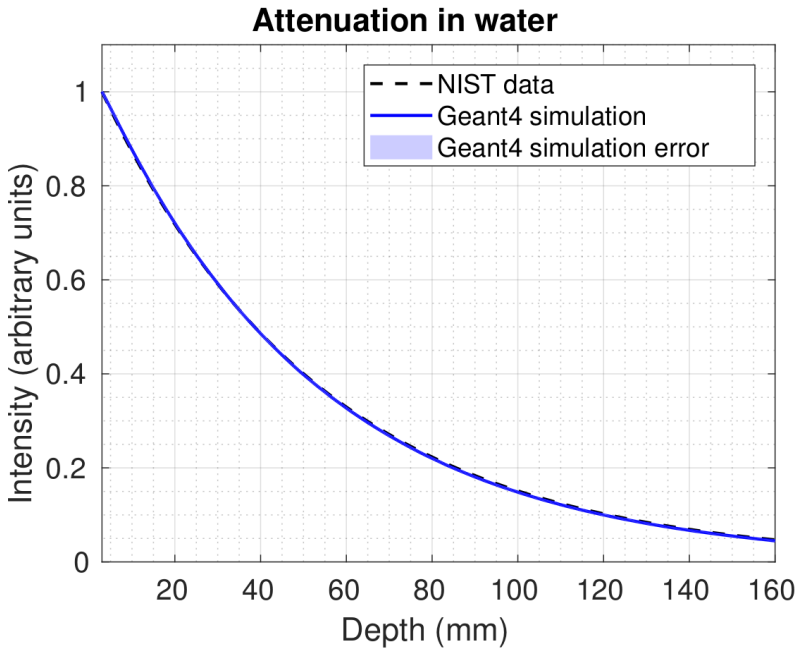

Figure 6.2: Theoretical and Geant4-simulated intensity in the simulation 1 as a function of depth for a 70 keV monoenergetic pencil beam with $2.4*10^9$ photons in a water-filled sphere surrounded by air. The data is normalised at a maximum that is set to 1, and it is shown from 3 mm to 160 mm. Error bars of the simulation are not visible since they are negligible at this scale.

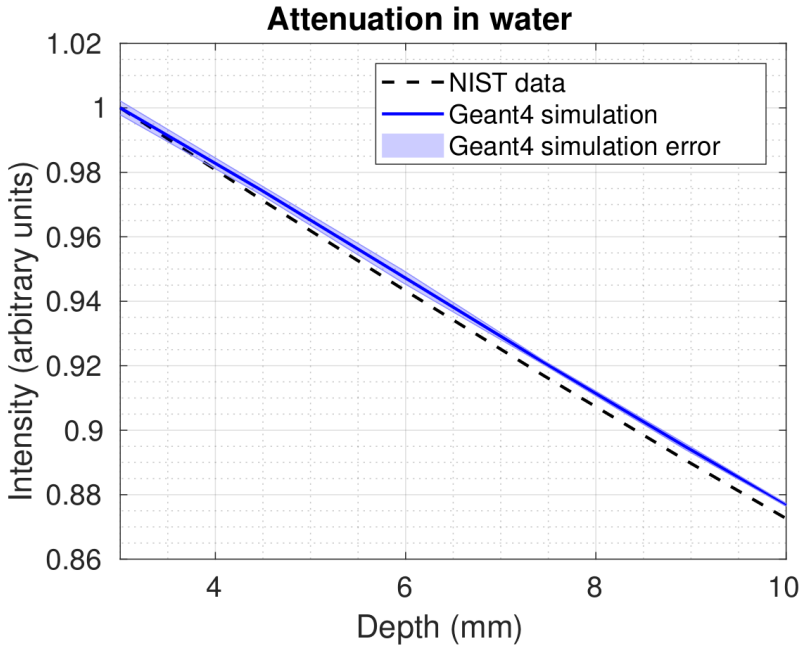

Figure 6.3: The data of Fig. 6.2 from the depth of 3 mm to the depth of 10 mm. Theoretical and Geant4-simulated intensity in the simulation of a 70 keV monoenergetic pencil beam with $2.4*10^9$ photons in a water-filled sphere surrounded by air. The data is normalised at a maximum that is set to 1. The Matlab code for the shaded error bars is from elsewhere [81].

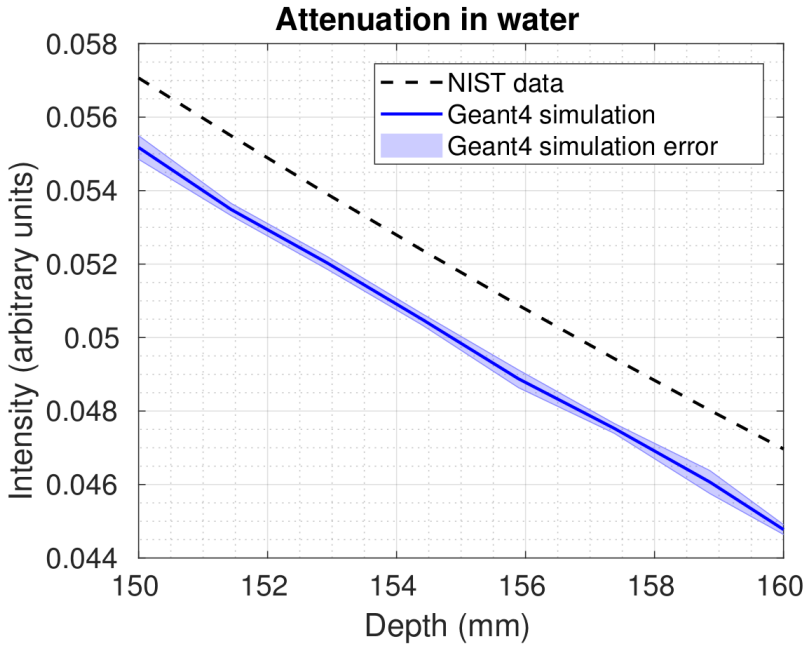

Figure 6.4: The data of Fig. 6.2 from the depth of 150 mm to the depth of 160 mm. Theoretical and Geant4-simulated intensity in the simulation 1 for a 70 keV monoenergetic pencil beam with $2.4*10^9$ photons in a water-filled sphere surrounded by air. The data is normalised at a maximum that is set to 1. The Matlab code for the shaded error bars is from elsewhere [81].

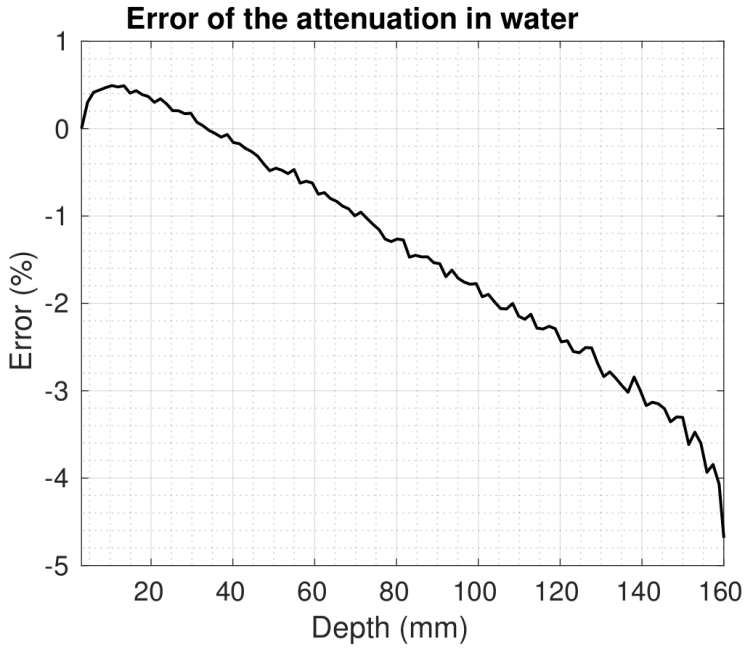

Figure 6.5: The difference of theoretical and Geant4-simulated intensity in the simulation 1 for a 70 keV monoenergetic pencil beam with $2.4*10^9$ photons in a water-filled sphere surrounded by air. The data is shown from 3 mm to 160 mm.

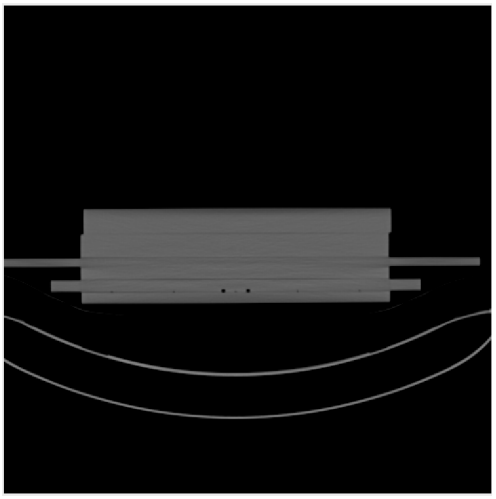

(a) The CT DICOM image for the simulation in polymethyl methacrylate (PMMA).

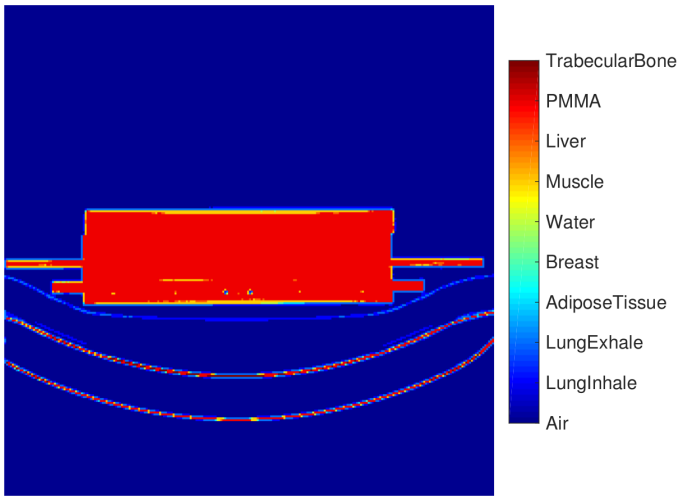

(b) Classification of materials and tissues of Fig. 6.6a performed with the DICOM program.

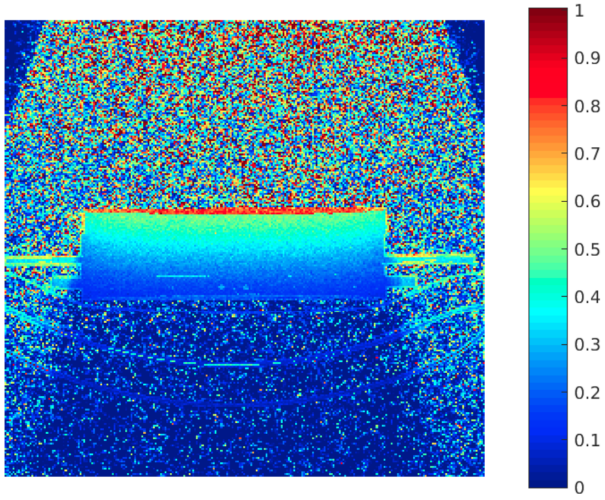

(c) Voxel-wise dose distribution for one of the 10 batches ($2*10^9$ photons) simulated with the DICOM program by using the materials and tissues of Fig. 6.6b (arbitrary units).

Figure 6.6: The centre slice of the plate image in the Geant4 simulation (simulation 2) of polymethyl methacrylate plates. CT refers to computed tomography and DICOM to digital imaging and communications in medicine.

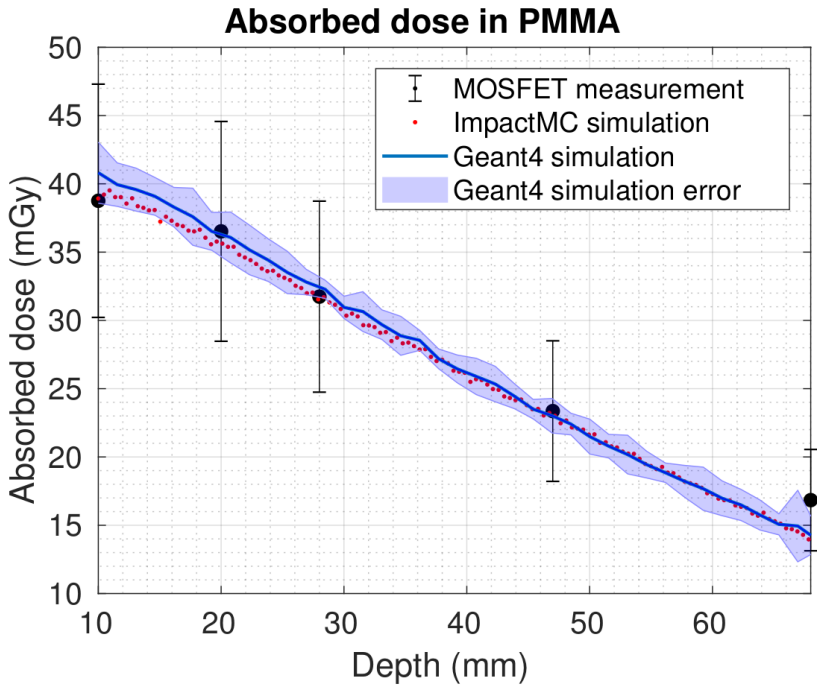

Figure 6.7: Measured and simulated absorbed dose as a function of depth for a diagnostic fan beam in polymethyl methacrylate surrounded by air. Simulations were performed with Geant4 (simulation 2) and ImpactMC (simulation 3). For the measurements, the 3σ error bars were calculated from the MOSFET calibration. The statistical uncertainty of the Geant4 simulation is a 3σ deviation between 10 simulation batches. ImpactMC does not give measures for statistical uncertainty. The Geant4 simulation was normalised to the second measurement point, and the ImpactMC simulation was normalised independently. MOSFET refers to metal-oxide-semiconductor field-effect transistor. The Matlab code for shaded error bars is from elsewhere [81].

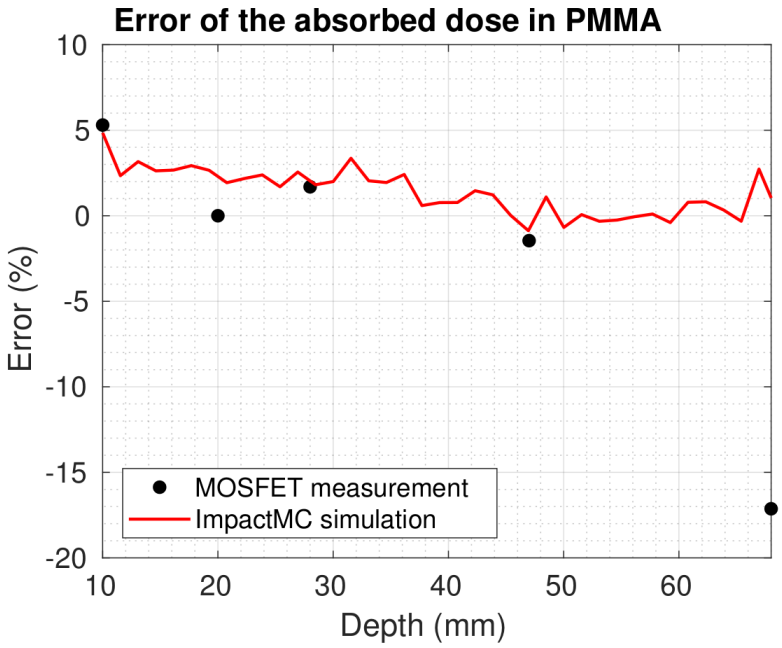

Figure 6.8: The difference of the Geant4 simulated absorbed dose in polymethyl methacrylate (PMMA, simulation 2) compared to the measured absorbed dose and to the ImpactMC simulation (simulation 3) for the data shown in Fig. 6.7.

ments. However, in X-ray energies, absorbed dose is approximately equal to air KERMA [82], and absorbed dose from the Geant4 simulation could be compared to the air KERMA from the measurements.

The ImpactMC simulation was normalised based on measurements with Siemens Somatom Edge. The air KERMA was 17.5 mGy/100 mAs, and hence the conversion factor was 0.035 (personal communication related to Euramet Empir project 15HLT05 on December 18, 2018). The ImpactMC results were converted to the absorbed dose in air, such that they are comparable to the MOSFET measurements that were calibrated in air.

The measured and simulated attenuation curves had approximately similar slope (Fig. 6.7). Although photon attenuation in general is exponential, it is approximately linear from the surface to the depth of 70 mm with the used energy spectrum. With the used normalisation, the MOSFET measurements deviated from the two simulations at a depth of 68 mm, and the Geant4 simulation deviated slightly from the MOSFET measurement and the ImpactMC simulation at a depth of 10 mm. The largest difference between the Geant4 simulation and the MOSFET reference was 17 % (2.5 mGy) and between the Geant4 simulation and the ImpactMC simulation 5 % (2.0 mGy, Fig. 6.8). However, all simulation results were within 3σ error bars. The MOSFET and ImpactMC simulation curves were not fully linear close to the surface like the Geant4 simulation curve. The dark artefact in the original CT image of the Geant4 simulation was in the same location (Fig. 6.6).

7. Discussion

In this project, the Geant4-based tool DICOM was modified for absorbed dose simulation in an X-ray projection imaging geometry for multiple input images. These modifications allowed configuration of parameters without a need to change the code and improved the ease of use when performing several simulations. Technically, importing DICOM images, applying a calibration curve, classifying materials and creating a voxelised phantom succeeded. In the project, the simulator was set up on a computer cluster, and a detailed description of the simulator and the use of the cluster was produced for the next developer.

In the calculation time tests, the only navigation method with a reasonable calculation time and reliable for our geometry was nested parameterisation. However, that navigation method could not be used in the Alcyone cluster due to incompatible software. The reason is probably a defect in the implementation of nested parameterisation of the DICOM simulator or a missing library in the Alcyone cluster. The defect will be investigated more closely in further research. In addition to the challenges on the cluster, nested parameterisation had minor challenges also in the Z600 computer when launching the simulator. However, these challenges did not prevent simulation in the Z600 computer. The simulator worked in the cluster with the other navigation methods except for with nested parameterisation. Therefore, Alcyone could have been used in the simulations of this project, but simulation times with other navigation methods would have been long. The used DICOM program was from the Geant4 package 10.3, and for future research it is worth investigating if the newer DICOM version in the Geant4 10.4 works better with the cluster.

The simulation of a narrow monoenergetic X-ray beam in water (simulation 1) showed a good agreement with theory, having the difference of 5 % in intensity compared to the reference. Smaller percentual statistical uncertainties could have been obtained if normalisation would have been performed deeper in water instead of the maximum of the curve. The error bars calculated as 3σ deviations from separate simulated batches were small, and they did not overlap everywhere with the theoretical reference curve. The lack of overlap could be further investigated. First, a correct method for calculation of the statistical uncertainty of the simulation could be reconsidered. In this project, the method suggested in the manual of the Penelope tool [17] produced a negligible statistical uncertainty, although clear fluctuation was visible in the simulated data. Therefore, error bars were not plotted according to this suggestion but as 3σ deviations from separate simulated batches. An appropriate number of simulation batches could be studied more deeply. In addition, other possible methods for the calculation of statistical uncertainty could be checked. Secondly, atomic cross section tables for water used by Geant4 could be

explored, and other physical models, such as Penelope or Livermore lists of Genat4, could be tested to further improve the result.

While theory is limited to ideal conditions, MOSFET detectors offered a practical method for reference measurements with a clinical set-up. MOSFETs were used in measuring the absorbed dose of a diagnostic X-ray beam as a function of depth in PMMA. In these measurements, the Geant4 simulation (simulation 2) showed the worst case difference of 17 % from the MOSFET measurements. It is worth noting that differences are substantially affected by normalisation. However, despite the relatively large difference, the simulation curve and measurement points were within the 3σ error bars. A disadvantage of the available MOSFETs was their low sensitivity, which increased the uncertainty of the reference. More accurate reference measurements could be obtained if high sensitivity MOSFETs recommended for radiology [78] were available or if a different type of reference, such as an ionisation chamber, was used. Geant4 simulation results were within 5 % from the second reference, ImpactMC simulation (simulation 3).

Calibration of MOSFETs in air is a possible source of uncertainty for MOSFETs, since different scatter characteristics were present in the MOSFET calibration and measurements. The calibration was performed in air, and therefore practically no scatter was present, while PMMA caused scatter in the measurement. The angular dependence of the MOSFET detectors may therefore have affected the measured dose, when scatter from multiple angles is present. In addition, scatter characteristics may be different at different depths in PMMA, which may lead to nonlinearity in the measured absorbed dose as a function of depth. In future research, MOSFET calibration and measurements could be performed in similar conditions, or factors correcting the possible inaccuracy could be used. The use of an ionisation chamber as a reference could also be considered, as mentioned earlier. The effect of scatter could be investigated by using Monte Carlo simulation.

MOSFETs were used for measuring dose as a function of depth in PMMA, and for practical reasons, the normalisation of the Geant4 simulation (simulation 2) was based on the same measurements. MOSFETs had been calibrated by using an ionisation chamber. In future measurements, the dose level could be determined independently from MOSFETs by measuring and simulating dose directly with an ionisation chamber.

The slight deviation of the Geant4 data (simulation 2) from the MOSFET and ImpactMC (simulation 3) data sets at a depth of 10 mm in PMMA may have been caused by the CT artefact near the surface of the PMMA plates. Lower HU values near the surface lead to classification of PMMA as tissues with a lower density, especially as muscle tissue. PMMA and muscle tissue contain essentially hydrogen, carbon and oxygen, while their proportions are different. In addition, muscle tissue contains small amounts of other elements, 4.3 % defined in the DICOM tool. These differences in the amounts of elements could have caused the little deviation from the references. ImpactMC and Geant4 simulations were performed with a similar CT image, where the same dark artefact was present. However, ImpactMC classified material into air, PMMA, carbon and lead. Therefore, materials having slightly lower HU values than those of PMMA were still classified as PMMA. That may explain little differences between Geant4 and ImpactMC simulations. The CT artefact does not necessarily affect ImpactMC simulations, while accurate calculation of

materials in Geant4 would make it sensitive to image artefacts. Another difference between the Geant4 and ImpactMC simulations was that Geant4 calculated electron transport and ImpactMC did not. However, the effect of electron transport is small in X-ray energies.

The correct X-ray energy spectrum and geometry are essential in simulation. The used diagnostic X-ray energy spectrum was created according to the HVL given by Siemens and evaluated using the SpekCalc program. The focus - plate surface distance, collimation and beam angle were simulated carefully according to scanner parameters. However, approximations of focus size, bowtie filter and angular beam properties are sources of uncertainty. More accurate results could be obtained if more information about the used CT scanner was available. With additional information about the X-ray tube, the spectrum could be simulated with Geant4. Simulation of a spectrum starting from electrons is a computationally demanding method. However, it is sufficient to simulate the spectrum with each X-ray tube geometry and peak energy once, as the photons created in the simulation can be saved to a phase-space file and read from that file whenever a new simulation is performed.

Previous Geant4 simulations of CTDI dose had uncertainty of 6 % [38], while the validation of the ImpactMC tool yielded uncertainty of 10 % [9]. Uncertainty of 20 % has been considered good in complex simulations such as CT dose simulation [9]. In this project, the set-up was a simple set-up of one projection, and thus the result could be expected to be more accurate than 17 %. According to the code of practice of the International Atomic Energy Agency (IAEA), the accuracy of 20 % is sufficient in estimating the absolute risk for stochastic effects in diagnostic radiology of adults, when radiation dose is relatively low [83]. Therefore, the results of this study are sufficiently accurate for that purpose. However, the code of practice also states that the lower level of 7 % error is required if deterministic effects are considered or if relative risk between different technologies is investigated. These are purposes of this simulator development, and therefore effort is required to decrease the uncertainty.

Simulations performed in this project took several days to complete although they were performed in eight parallel CPU cores. Use of the cluster would speed up simulations if the necessary amount of CPU cores were available. Geant4 permits multi-threaded calculation that could possibly be configured to the cluster. Alternatively, scripts could be written for sending calculation to several queues to avoid an excessive manual work. When using a cluster, necessary calculation resources must be guaranteed, since the simulator requires dozens of CPU cores for fair simulation times. The choice of a navigation method appeared to be important for both speed and accuracy. Instead, changing the cut range did not change the calculation time in practice. Another possibility for faster calculation would be graphics processing unit (GPU) calculation. Geant4 does not support calculation with a GPU, but some Geant4 users have improved simulation times by creating their own GPU calculation for Geant4, and they have also optimised the code for medical physics [84]. That development work was performed for radiotherapy, but similar improvements could be performed for this diagnostic X-ray dose simulator. GPU calculation would be available in the Alcyone cluster. Alternatively, simulation of secondary electrons is not necessarily required in diagnostic X-ray physics. In this first step of the simulator development, electron transport was calculated. Next, influence of electron

transport on results and computation time could be investigated. Particle cut ranges could also be examined more in detail.

The DICOM program from Geant4 is a workable base for creating a diagnostic X-ray simulator, and Geant4 offers nearly unlimited possibilities for development. However, although the code is implemented in C++, it may be challenging for a new developer to understand it. For efficient use of Geant4 and the simulator, proficient programming skills are a requirement. In addition, the DICOM program includes defects which affect the usage of the tool. Correction of most defects was out of the scope of this project but will be necessary in future.

The first version of the simulator described here can simulate dose in a simple planar X-ray imaging geometry such as the geometry used in conventional X-ray. In future, the use of the simulator could be broadened for other X-ray applications such as CT and CBCT by adding rotation and a bowtie filter. Present simulations were performed in a phantom, but there is no technical reason for not simulating dose in a patient. Simulation of patients would allow calculation of individual radiation dose and optimisation of X-ray imaging with different anatomies.

8. Conclusions

The Geant4 DICOM tool is a versatile tool that can be used to simulate absorbed dose in planar X-ray imaging. The simulation results compared to theory showed an accuracy of 5 %, while the simulation closer to a clinical situation yielded a maximal difference of 17 %. However, the author believes that the DICOM tool has a potential for more accurate results than that. The used standard-sensitivity MOSFET detectors had an unacceptable level of variation to serve as a reference, and more sensitive detectors are necessary for the used dose level. The results of the diagnostic X-ray beam agreed with ImpactMC simulation with a difference of 5 %. Part of the difference of the Geant4 simulation compared to the references may also be due to sensitivity of the DICOM tool to CT artefacts, due to MOSFET calibration and due to spectrum modelling.

The technical modifications performed for the tool in this project will help a user to accomplish conveniently several simulations in varied geometries. However, the tool has a few critical challenges, the greatest being incompatibility of one of the navigation methods with the Alcyone cluster. For increased computational power, the use of a cluster is necessary. Calculation times could also be decreased by omitting electron transport, since it is most likely not required in keV energies of X-ray imaging. GPU calculation and optimising the code for medical physics would fasten simulations, but they require a considerable amount of work.

The tool has a great potential if the described limitations are addressed. The future use of the simulator requires further development of the program, especially with new imaging geometries. Possibilities for X-ray simulator development are broad with Geant4, however, the Geant4 code requires a skilled programmer team.

A. Simulator development

A.1 Source files

The source files for the simulator (Table A.1) include files from different Geant4 examples, other files from the Geant4 package and files added by the author. The Geant4 package provides examples that have been modified and combined for this project [19, 60]. Names of the original Geant4 files have been kept for traceability:

- *B2* refers to the B2 example in the Geant4 package.
- *Dicom* refers to the DICOM example.
- The files starting with *G4* and the file PhysListEmStandard are from the physics lists shared in the Geant4 package [60].
- PhysicsList, PhysicsListMessenger, StepMax and StepMaxMessenger are from the TestEm2 example in the electromagnetic section of the package.

The files were modified to serve this simulator, and some bugs were fixed. ReadIni was created during the development of this simulator. The colour of materials mentioned in some source files refers to colours in Geant4 visualisation which is, however, not used in the cluster. In addition to these files, the main file DICOM.cc starts the simulation and controls all action.

A.2 Development of the Geant4 DICOM project

The simulator was built mainly based on the DICOM example. The author of this work has developed the DICOM program further and set it up to the Alcyone cluster. A list of developments include

- creating the geometry of an X-ray beam and a patient
- methods to handle hundreds of image slices instead of three
- fixing bugs in the DICOM program related to reading of slices
- adding the Mersenne Twister pseudorandom number generator
- creating a diagnostic X-ray spectrum
- adding several physical models
- defining a more versatile particle gun (the Geant4 General Particle Source instead of the Geant4 Particle Gun)
- using a timestamp as a seed of simulation and as a folder name for results
- changing parameter handling and result saving from hardcoded commands to parameter files (parameters in Data.dat were also moved to ini.txt and results to files dose.txt in the timestamp folder)

Table A.1: Source (.cc) and included (.hh) files of the simulator.

File name	Description
DICOM	The main file.
B2TrackerHit	Stores information about charged particles in a selected volume.
B2TrackerSD	Processes hits.
DicomActioninitialisation	Initialises processes.
DicomDetectorConstruction	Constructs the geometry, makes materials, creates the simulation world and reads DICOM data.
DicomEventAction	Controls the beginning and the end of an event.
DicomHandler	Handles DICOM files and makes g4dcm files.
DicomIntersectVolume	Manages intersections of DICOM files and volumes.
DicomNestedParamDetectorConstruction	Constructs the detector for the nested parameterisation method (not used by default with the simulator).
DicomNestedPhantomParameterisation	Auxiliary class for nested parameterisation.
DicomPartialDetectorConstruction	Creates an intersection of a phantom and a volume if chosen.
DicomPhantomParameterisationColour	Gives colour to each material if OpenGL visualisation is used.
DicomPhantomZSliceHeader	Contains slice information.
DicomPhantomZSliceMerged	Merges slices to form a volume.
DicomPrimaryGeneratorAction	Generates photons.
DicomRegularDetectorConstruction	Constructs the detector used in the methods 1D and 3D optimisation and regular navigation.
DicomRun	Collects information such as dose from events and forms run information.
DicomRunAction	Controls the beginning and the end of a run and saves dose to files.
DicomSteppingAction	Action at each step, collects data for a beam test.
G4EmLivermorePhysics	Constructs low energy physics using Livermore data.
G4EmPenelopePhysics	Constructs low energy physics using Penelope data.
G4EmStandardPhysics_option4	Constructs low and intermediate energy physics.
PhysicsList	Controls the use of physical models.
PhysicsListMessenger	Auxiliary class for physical models.
PhysListEmStandard	A physical model used by the original DICOM example.
ReadIni	Reads parameters from ini.txt.
StepMax	Auxiliary class for physical models.
StepMaxMessenger	Auxiliary class for physical models.

- modification of memory usage
- setting up the simulator to the cluster in the University of Helsinki
- analysing and visualising the results with Matlab and
- writing detailed instructions for setting up the simulator and using it at the cluster or an individual computer.

A.3 Known issues

The issues to be fixed in the simulator include:

- When slices are merged, the following error may be printed to the log: "DicomPhantomZSliceMerged::CheckSlices - Slice Distance Error in slice [386]: Real Distance = 2.5 mm, Stated Distance = 2.5 mm". The simulator is however started normally.
- When launching the simulator and if nested parameterisation is in use, sometimes the program gets stuck in "Constructing DicomNestedPhantomParameterisation", and the use of memory increases. In this case the simulator must be launched again.
- With nested parameterisation, simulation causes segmentation fault in the Alcyone cluster, but the same has not happened in the individual computer (Z600).
- Multi-treading configuration does not work in the Alcyone cluster or has not been configured properly. Manual multi-threading can be used by sending simulation to several calculation queues.
- If a calibration curve different from the default calibration curve is configured, the following error is printed and G4dcm files are not created: @@@ Error density = -1.000000 && Pixel = -1007 (0xfffffc11) && deltaDensity/deltaCT = -nan.

A.4 Further development of the simulator

Possible further developments include

- Fixing the known issues listed in App. A.3.
- Error analysis in the case of wrong parameters.
- Program code to import DICOM images with any names to the simulator. Currently the imported images must be numbered correctly.
- Providing a fan beam or a cone beam with a square cross section without collimators created as geometrical objects.
- Creating the CT geometry with irradiation from multiple angles and a bowtie filter.
- Simulating an energy spectrum with Geant4 if exact parameters of the X-ray tube are known.
- Measuring the calibration curve for the CT used in the reference measurements.

B. Simulator instructions

B.1 Setting up Geant4 on the Alcyone cluster

Geant4 is already installed on the Alcyone cluster of the University of Helsinki, and it is easily set up with a few commands. Setting up Geant4 is shown here for Geant4 version 4.10.1p1 on the Alcyone cluster. The Geant4 User's Guide for Application developers [65] can be referred to for further information.

To choose the correct software versions, add the following commands to the shell script `.bashrc` in the home folder:

```
module add cmake
module add gcc/4.9.2
source /cvmfs/fgi.csc.fi/apps/sl6/geant4/4.10.1p1/bin/geant4.sh
```

The following message can be ignored: "Please load PrgEnv-gnu first, but loading anyway".

Next, copy the project folder, for example `simulator`, to your folder, in this example `/home/user/`. Here the build folder was created under the `simulator` folder:

```
[user@alcyone simulator]$ mkdir build
```

In the build folder, run cmake to use the correct C and C++ compilers:

```
[user@alcyone build]$ cmake -DCMAKE_C_COMPILER=/cvmfs/fgi.csc.fi/
compilers/sl6/gnu/gcc/4.9.2/bin/gcc -DCMAKE_CXX_COMPILER=/cvmfs/fgi.
csc.fi/compilers/sl6/gnu/gcc/4.9.2/bin/g++
```

Run cmake again to create make files. `Geant4\_DIR` defines the path of the Geant4 installation folder, and the second argument is the source folder of the project:

```
[user@alcyone build]$ cmake -DGeant4_DIR=/cvmfs/fgi.csc.fi/apps/sl6/
geant4/4.10.1p1/lib64/Geant4-10.1.1/ /home/user/simulator/
```

To build C++ objects and to create the executable:

```
[user@alcyone build]$ make
```

The executable can now be launched (App. B.4) if the parameters have been configured (App. B.2). When changes have been made to the code, run again `make`. When new files have been added, re-run `cmake -DGeant4_DIR=...`

B.2 Parameters

Before launching the simulator, multiple parameters must be provided. The structure of the simulator is described in Ch. 4.1. The parameter files include

- Calibration curve: calibrationCurve.txt
- Tissue densities: tissues.txt
- The Geant4 macro file: a name decided by the user
- Initialisation file: ini.txt
- A SLURM file: a name decided by the user

The described parameter files must be located in the configuration folder (see App. B.2.4), where the simulation is launched, except for the tissue density file, which is located with the corresponding DICOM image set in the data folder. These parameter files are described in App. B.2.1-B.2.4. In addition, the user must choose a voxel navigation method (App. B.2.5).

B.2.1 Calibration curve

A calibration curve (calibrationCurve.txt) defines how HU values are converted into material densities. The first row includes the number of data points. The following rows include an HU value and the corresponding density value in mg/cm^3 in ascending order, as described in Table B.1.

Table B.1: An example of the file calibrationCurve.txt: HU values (on the left) and tissue densities in mg/cm^3.

8	
-5000	0.0
-1000	0.0
-400	0.602
-150	0.924
100	1.075
300	1.145
2000	1.856
4927	3.379

B.2.2 Tissue densities

Tissue densities (tissues.txt) are related to the particular image set, and the file is therefore placed in the data folder with DICOM images. Each tissue is classified with a density range. The first row of the file is the number of tissues, while the

following rows represent the material followed by its upper density limit in mg/cm^3 (Table B.2). For example, the density of a liver ranges from the limit of muscle tissue (1.109 mg/cm^3) to the limit 1.113 mg/cm^3. The lower limit of the first material is zero.

Table B.2: The file tissues.txt defining tissue densities in mg/cm^3.

10	
Air	0.207
LungInhale	0.481
LungExhale	0.919
AdiposeTissue	0.979
Breast	1.004
Water	1.043
Muscle	1.109
Liver	1.113
TrabecularBone	1.496
DenseBone	1.654

B.2.3 Macro file

The macro file uses Geant4's macro commands to define the simulation. Many commands can be given through a macro file without the need to modify the code. Two example macro files are given in App. B.6 and App. B.7.

B.2.4 Initialisation file

The aim of creation of the initialisation file was to decrease the need to modify the code. The parameters that were not defined in the other parameter files are configured in ini.txt (Table B.3). Ini.txt is read by the ReadIni.cc (App. A.1). Care must be used when modifying the initialisation file since error handling does not necessarily recognise all mistakes, and the error message may not be informative.

B.2.5 Voxel navigation

If no configuring is done, the simulator uses the fast version of regular navigation (Ch. 4.6, option 4A). Option 4B was not implemented in the Geant4's DICOM example code [19]. Optimisation in a 3D grid (option 1) is used by setting `phantom_phys->SetRegularStructureId(0)` in DicomRegularDetectorConstruction.cc. 1D optimisation (1) is not recommended due to the long computation time. Nested parameterisation (option 3) is used by setting an environment parameter in the command line before launching the simulator: `export DICOM_NESTED_PARAM=1`. The command can also be added to `.bashrc`. Configuration of the environment parameter is checked with the command `env`.

Table B.3: Parameters in ini.txt. If a parameter has a certain number of options, they are indicated in the description. A row is commented with #. The file should not have empty lines.

Parameter	Type	Description	Example value
numberOfThreads	G4double	The number of CPU cores in multi-threaded calculation.	8
dataFolder	G4String	The path for DICOM data and tissues.txt (Table B.2). The path must end with "/".	/home/user/geant4/data/
dataSetName	G4String	The name of the DICOM folder placed in the data folder. The path must end with "/".	levyt/
configuration-Folder	G4String	The path for the executable file and parameter files. The path must end with "/".	(Empty)
resultsFolder	G4String	The path where the result folder of each simulation named after the timestamp is saved. The path must end with "/".	/home/user/geant4/results/
checkGeometry-Overlaps	G4double	Defines if geometry overlap is checked. Options: 0, 1.	1
colZ1PosX	G4double	Collimator 1 position in X (mm).	0
colZ1PosY	G4double	Collimator 1 position in Y (mm).	492
colZ1PosZ	G4double	Collimator 1 position in Z (mm).	86
colZ1SizeX	G4double	Collimator 1 size in X (mm).	300
colZ1SizeY	G4double	Collimator 1 size in X (mm).	3
colZ1SizeZ	G4double	Collimator 1 size in X (mm).	200
colZ2PosX	G4double	Collimator 2 position in X (mm).	0
colZ2PosY	G4double	Collimator 2 position in Y (mm).	492
colZ2PosZ	G4double	Collimator 2 position in Z (mm).	-123
colZ2SizeX	G4double	Collimator 2 size in X (mm).	300
colZ2SizeY	G4double	Collimator 2 size in Y (mm).	3
colZ2SizeZ	G4double	Collimator 2 size in Z (mm).	200
colZ2Mat	G4String	Collimator material. Must use Geant4's material codes.	G4_Pb
compression	G4double	A compression factor of DICOM images for a voxelised model.	2
imageName	G4String	The first letters of DICOM image names.	IMG0
imageType	G4String	The ending of the image type. Options: IMA, dcm.	IMA
firstImageNumber	G4double	The number of the first DICOM image.	1
lastImageNumber	G4double	The number of the last DICOM image.	101
worldAirDensity	G4double	The air density in mg/cm^3 used around the voxelised volume.	1.290
physicsList	G4String	Physical models. Options: emstandard_opt4, emlivermore, empenelope.	emstandard_opt4

B.3 Geant4 DICOM files

Geant4 DICOM files (with the endings g4dcm and g4dcmb) are used for creating a voxelised model. The simulator creates them from DICOM files when launching the

simulator. They are text files with the following information, with each item in the list starting a new line [19]

- the number of materials
- the index and name of each material
- the number of voxels (X, Y and Z)
- the minimum and maximum extension in X (mm)
- the minimum and maximum extension in Y (mm)
- the minimum and maximum extension in Z (mm)
- several lines containing the nVoxelX*nVoxelY*nVoxelZ material indices (one per voxel) and
- several lines containing the nVoxelX*nVoxelY*nVoxelZ material densities (one per voxel).

B.4 Running the simulator with a computer

When the required parameter files (App. B.2) have been configured, the simulator is simply launched in the run folder by

```
./DICOM
```

The program is ready for simulation, when text `Idle>` appears. A run is started with a macro file:

```
/control/execute/run.mac
```

B.5 Running the simulator with SLURM

The simulator is run on a cluster, in this case Alcyone, by using SLURM Workload Manager [70]. To run a job, write a file, for example run.sh that includes the following lines:

```
#!/bin/bash
#SBATCH -N 1
#SBATCH -n 12
#SBATCH -J run1
#SBATCH -e e1.err
#SBATCH -p 8G_short_ser
#SBATCH -t 7-00:00:00
./DICOM /scratch/user/run/run.mac
```

Then run it:

```
sbatch run.sh
```

SLURM commands can be found in [70]. During simulation, a slurm-*.out file including simulator prints is saved to the home folder. Results are saved to the results folder defined in ini.txt.

Notice that nested parametrisation cannot be used in the Alcyone cluster with the current configuration (Ch. A.3).

B.6 Macro file for simulation with a monoenergetic X-ray beam with Geant4 (simulation 1)

Simulation with a monoenergetic pencil beam is shown below for the geometry used in the simulation (Ch. 5.2) for $2 * 10^8$ photons.

```
/gps/ene/mono 70 keV

/gps/position 0 657.5 -190 mm

/gps/pos/type Beam

/gps/direction 0 -1 0

/run/setCutForAGivenParticle gamma 1.0 mm
/run/setCutForAGivenParticle e- 1.0 mm

/run/beamOn 200000000
```

B.7 Macro file for simulation with a diagnostic X-ray spectrum with Geant4 (simulation 2)

Simulation with an energy spectrum is shown below for the geometry used in the simulation (Ch. 5.3.2) for $2 * 10^8$ photons.

```
/gps/ene/type User
/gps/hist/type energy

/gps/hist/point 0.0125 1.814134e-12
/gps/hist/point 0.013 2.468984e-10
/gps/hist/point 0.0135 9.689549e-09
/gps/hist/point 0.014 3.843773e-07
/gps/hist/point 0.0145 6.160301e-06
/gps/hist/point 0.015 0.0000996
/gps/hist/point 0.0155 0.0008632
/gps/hist/point 0.016 0.0075478
/gps/hist/point 0.0165 0.0404413
/gps/hist/point 0.017 0.2182233
```

...
(The definition of the histogram continues until the peak energy.)

```
/gps/position 0 633 408 mm

/gps/ang/type iso

/gps/ang/mintheta 159.5 deg
/gps/ang/rot1 1 0 0
/gps/ang/rot2 0 0 1

/run/setCutForAGivenParticle gamma 1.0 mm
/run/setCutForAGivenParticle e- 1.0 mm

/run/beamOn 200000000
```

Bibliography

[1] Paile, W. *Säteily- ja ydinturvallisuus: Säteilyn terveysvaikutukset.* Säteilyturvakeskus, 2002.

[2] Järvinen, H. *Terveydenhuollon säteilyn käytöstä (röntgendiagnostiikka ja toimenpideradiologia) väestölle aiheutuvan säteilyannoksen määrittäminen.* Säteilyturvakeskus, STUK-TR 21, 2016.

[3] Suutari, J. *Radiologisten tutkimusten ja toimenpiteiden määrät vuonna 2015.* Säteilyturvakeskus, STUK-B 207, 2016.

[4] Kalender, W. A. Dose in x-ray computed tomography. *Phys. Med. Biol.*, 59:R129–R150, 2014.

[5] Lell, M. M., Wildberger, J. E., Alkadhi, H., Damilakis, J. and Kachelriess, M. Evolution in computed tomography: the battle for speed and dose. *Investigative Radiology*, 00(00), 2015.

[6] Massera, R. T. and Tomal, A. Skin models and their impact on mean glandular dose in mammography. *Physica Medica*, 51:38–47, 2018.

[7] McCollough, C. H., Leng, S., Yu, L., Cody, D. D., Boone, J. M. and McNitt-Gray, M. F. CT Dose Index and Patient Dose: They Are Not the Same Thing. *Radiology*, 259(2), May 2011.

[8] Dedulle, A., Fitousi, N., Zhang, G., Jacobs, J. and Bosmans, H. Two-step validation of a Monte Carlo dosimetry framework for general radiology. *Physica Medica*, 53:72–79, 2018.

[9] Deak, P., van Straten, M., Shrimpton, P., C., Zankl, M. and Kalender, W. A. Validation of a Monte Carlo tool for patient-specific dose simulations in multi-slice computed tomography. *Eur. Radiol.*, 18(759-772), 2008.

[10] CT Imaging. *User Guide - ImpactMC, version 1.20.* 2010-2016.

[11] Andersen, E. Monte Carlo dose simulator for diagnostic x-ray. Program code and document in GitHub. https://github.com/medicalphysics/OpenDXMC, latest commit 20.10.2017, referred 14.8.2018.

[12] Tapiovaara, M. and Siiskonen, T. *PCXMC. A Monte Carlo program for calculating patient doses in medical x-ray examinations, STUK-A231, 2nd Ed.* Säteilyturvakeskus, November 2008.

[13] Werner, C. J.(editor). *MCNP (TM) User's Manual Code Version 6.2*. Los Alamos National Laboratory Technical Report LA-UR-17-29981, 2017.

[14] Nelson, W. R., Hirayama, H. and Rogers, D. W. O. *The EGS4 Code System*. Stanford Linear Accelerator Center, Stanford University, SLAC-265 UC-32, December 1985.

[15] Hirayama, H., Namito, Y., Bielajew, A. F., Wilderman, S. J. and Nelson, W. R. *The EGS5 Code System*. Stanford Linear Accelerator Center, Stanford University, SLAC-R-730, December 2005.

[16] Kawrakow, I. Accurate condensed history Monte Carlo simulation of electron transport. I. EGSnrc, the new EGS4 version. *Med. Phys.*, 27(3):485–498, March 2000.

[17] Salvat, F., Fernandez-Varea, J. M. and Sempau, J. Penelope-2011: A code system for Monte Carlo simulation of electron and photon transport. *Workshop Proceedings*, 2011.

[18] Agostinelli, S., Allison, J., Amako, K. et al. Geant4 - A Simulation Toolkit. *Nuclear Instruments and Methods in Physics Research*, Section A(506):250–303, 2003.

[19] Geant4 Collaboration. Geant4 Example Documentation. http://geant4-userdoc.web.cern.ch/geant4-userdoc/Doxygen/examples_doc/html/index.html, last modified 15.1.2018, referred 20.5.2018.

[20] Andreo, P., Burns, D. T., Nahum, A. E., Seuntjens, J. and Attix, F. H. *Fundamentals of Ionizing Radiation Dosimetry*. John Wiley VCH, 2017.

[21] Bushberg, J. T., Seibert, J. A., Leidholdt, E. M. and Boone, J. M. *The Essential Physics of Medical Imaging*. Lippincott Williams and Wilkins, 2012.

[22] National Institute of Standards and Technology. Physical reference data. https://www.nist.gov/, referred 26.2.2019.

[23] Djurabekova, F. Basics of Monte Carlo simulations, course material, Helsinki University, spring 2018.

[24] Mellin, I. *Todennäköisyyslaskenta ja tilastotiede: Kaavat*. Course material, Helsinki University of Technology, 2006.

[25] Ioppolo, J. L., Price, R. I., Tuchyna, T. and Buckley, C. E. Diagnostic x-ray dosimetry using Monte Carlo simulation. *Phys. Med. Biol.*, 47:1707–1720, 2002.

[26] Kawrakow, I., Mainegra-Hing, E., Rogers, D. W. O., Tessier, F. and Walters, B. R. B. *The EGSnrc Code System: Monte Carlo Simulation of Electron and Photon Transport*. Technical Report PIRS-701, National Research Council Canada, 2018.

[27] Verhaegen, F. and Seuntjens, J. Monte Carlo modelling of external radiotherapy photon beams. *Phys. Med. Biol*, 48(21), 2003.

[28] Mendes, M., Costa, F., Figueira, C., Madeira, P., Teles, P. and Vaz, P. . Assessment of patient dose reduction by bismuth shielding in CT using measurements, Geant4 and MCNPX simulations. *Radiation Protection Dosimetry*, 165(1-4), 2015.

[29] Gu, J., Bednarz, B., Caracappa, P. F. and Xu, X. G. The development, validation and application of a multi-detector CT (MDCT) scanner model for assessing organ doses to the pregnant patient and the fetus using Monte Carlo simulations. *Phys. Med. Biol.*, 54:2699–2717, 2009.

[30] Myronakis, M., Perisinakis, K., Tzedakis, A., Gourtsoyianni, S. and Damilakis, J. Evaluation of a patient-specific Monte Carlo software for CT dosimetry. *Rad. Prot. Dos.*, 133(4), 2009.

[31] Ohno, T., Araki, F., Onizuka, R. et al. Comparison of dosimetric properties among four commercial multi-detector computed tomography scanners. *Physica Medica*, 35(50-58), 2017.

[32] Jarry, H., DeMarco, J. J., Beifuss, U., Cagnon, C. H. and McNitt-Gray, M. F. A Monte Carlo-based method to estimate radiation dose from spiral CT: from phantom testing to patient-specific models. *Phys. Med. Biol.*, 48:2645–2663, 2003.

[33] Li, X., Samei, E., Segars, W. P., Sturgeon, G. M., Colsher, J. G., Tocheva, G., Yoshizumi, T. T. and Frush, D. P. Patient-specific radiation dose and cancer risk estimation in CT: Part I. Development and validation of a Monte Carlo program. *Med. Phys.*, 38(1), January 2011.

[34] Pan, Y., Qiu, R., Gao, L., Ge, C., Zheng, J., Xie, W. and Li, J. Development of 1-year-old computational phantom and calculation of organ doses during CT scans using Monte Carlo simulation. *Phys. Med. Biol.*, 59:5243–5260, 2014.

[35] DeMarco, J. J. A Monte Carlo based method to estimate radiation dose from multidetector CT (MDCT): cylindrical and anthropomorphic phantoms. *Phys. Med. Biol.*, 50:3989–4004, 2005.

[36] DeMarco, J. J., Cagnon, C. H., Cody, D. D., Stevens, D. M., McCollough, C. H., Zankl, M., Angel, E. and McNitt-Gray, M. F. Estimating radiation doses from multidetector CT using Monte Carlo simulations: effects of different size voxelized patient models on magnitudes of organ and effective dose. *Phys. Med. Biol.*, 52:2583–2597, 2007.

[37] Huang, Y., Zhuo, W., Gao, Y. and Liu, H. Monte Carlo simulation of eye lens dose reduction from CT scan using organ based tube current modulation. *Physica Medica*, 48:72–75, 2018.

[38] Carver, D. E., Kost, S. D., Fernard, M. J., Lewis, K. G., Fraser, N. D., Pickens, D. R., Price, R. R. and Stabin, M. G. Development and validation of a GEANT4 radiation transport code for CT dosimetry. *Health Phys.*, 108(4):419–428, 2015.

[39] Li, X., Samei, E., Segars, W. P., Sturgeon, G. M., Colsher, J. G. and Frush, D. P. Patient-specific Radiation Dose and Cancer Risk for Pediatric Chest CT. *Radiology*, 259(3), June 2011.

[40] Li, X., Samei, E., Segars, W. P., Sturgeon, G. M., Colsher, J. G., Tocheva, G., Yoshizumi, T. T. and Frush, D. P. Patient-specific radiation dose and cancer risk estimation in CT: Part II. Application to patients. *Med. Phys.*, 38(1), January 2011.

[41] Kelaranta, A., Mäkelä, T., Kaasalainen, T. and Kortesniemi, M. Fetal radiation dose in three common CT examinations during pregnancy - Monte Carlo study. *Physica Medica*, 43:199–206, 2017.

[42] van Eeden, D. and du Plessis, F. EGS_cbct: Simulation of a fan beam CT and RMI phantom for measured HU verification. *Physica Medica*, 32(1375-1380), 2016.

[43] Kelaranta, A., Toroi, P. and Vock, P. Incident air kerma to absorbed organ dose conversion factors for breast and lung in PA thorax radiography: The effect of patient thickness and radiation quality. *Physica Medica*, 32:1594–1601, 2016.

[44] Siiskonen, T., Tapiovaara, M., Kosunen, A., Lehtinen, M. and Vartiainen, E. Monte Carlo simulations of occupational radiation doses in interventional radiology. *BJR*, 80:460–468, 2007.

[45] Zhang, G., Marshall, N., Bogaerts, R., Jacobs, R. and Bosmans, H. Monte Carlo modeling for dose assessment in cone beam CT for oral and maxillofacial applications. *Med. Phys.*, 40(7), July 2013.

[46] Stratis, A., Zhang, G., Lopez-Rendon, X., Jacobs, R., Bogaerts, R. and Bosmans, H. Customization of a Monte Carlo dosimetry tool for dental cone-beam CT systems. *Rad. Prot. Dos.*, 169(1-4):378–385, February 2016.

[47] Kyriakou, Y., Deak, P., Langner, O. and Kalender, W. A. Concepts for dose determination in flat-detector CT. *Phys. Med. Biol.*, 53:3551–3566, 2008.

[48] Munoz, I. D., Gamboa-deBuen, I., Avila, O. and Brandan, M. E. Dosimetry in a mammography phantom using TLD-300 dosimeters. *Med. Phys.*, 45(9), September 2018.

[49] Poludniowski, G. G., and Evans, P. M. Calculation of x-ray spectra emerging from an x-ray tube. Part I. Electron penetration characteristics in x-ray targets. *Med. Phys.*, 34(6), 2007.

[50] Poludniowski, G. Calculation of x-ray spectra emerging from an x-ray tube. Part II. X-ray production and filtration in x-ray targets. *Med. Phys.*, 34(6), 2007.

[51] Poludniowski, G., Landry, G., DeBlois, F., Evans, P. M. and Verhaegen, F. SpekCalc: A program to calculate photon spectra from tungsten anode x-ray tubes. *Physics in Medicine and Biology*, 54(19), 2009.

[52] Siewerdsen, J. H., Waese, A. M., Moseley, D. J., Richard, S. and Jaffray, D. A. Spektr: A computational tool for x-ray spectral analysis and imaging system optimization. *Med. Phys.*, 31(11):3057–3067, 2004.

[53] Cunha, D. M., Tomal, A. and Poletti, M. E. Monte Carlo Simulation of X-Ray Spectra in Mammography and Contrast-Enhanced Digital Mammography Using the Code PENELOPE. *IEEE Trans. Nucl. Med.*, 60(2), April 2013.

[54] Jiang, H. and Paganetti, H. Adaptation of Geant4 to Monte Carlo dose calculations based on CT data. *Med. Phys.*, 31(10):2811–2118, October 2004.

[55] Gholami, S., Longo, F., Nedaie, H. A., Berti, A., Mousavi, M. and Meigooni, A. S. Application of Geant4 Monte Carlo simulation in dose calculations for small radiosurgical fields. *Med. Dos.*, 43(3):214–223, 2018.

[56] Archambault, L., Beaulieu, L., Carrier, J. F. et al. Overview of Geant4 Applications in Medical Physics. *IEEE NSS/MIC*, pages 1743–1745, 2003.

[57] Allison, J., Amako, K., Apostolakis, J. et al. Geant4 Developments and Applications. *IEEE Trans. Nucl. Sci.*, 53(1), 2006.

[58] Allison, J., Amako, K., Apostolakis, J. et al. Recent Developments in Geant4. *Nucl. Instrum. Meth. A*, 835:186–225, 2016.

[59] Ivanchenko, V. N. Geant4: physics potential for instrumentation in space and medicine. *Nucl. Instrum. Meth. A*, 525:402–405, 2004.

[60] Geant4 Collaboration. Geant4.10.01.p03 package code. Available in https://geant4.web.cern.ch/support/download_archive.

[61] Amako, K., Guatelli, S., Ivanchencko, V. et al. Geant4 and its validation. *Nuclear Physics B (Proc. Suppl.)*, 150:44–49, 2006.

[62] Amako, K., Guatelli, S., Ivanchenko, V. N. et al. Comparison of Geant4 Electromagnetic Physics Models Against the NIST Reference Data. *IEEE Trans. Nucl. Sci.*, 52(4), August 2005.

[63] Geant4 Collaboration. Geant4 - A Simulation Toolkit. https://geant4.web.cern.ch/, referred 19.5.2018.

[64] CERN. Low Energy Electromagnetic Physics Working Group. https://new-geant4-dev.web.cern.ch/node/1615, referred 12.10.2018.

[65] Geant4 Collaboration. Geant4 User's Guide for Application Developers. Geant4 version 10.3, 9.12.2016.

[66] Italian National Institute for Nuclear Physics (INFN). Geant4 Tutorial course. Physics in Geant4: Particles, processes, cuts and models, course material 6-10 July 2015 GSSI, L'Aquila, Italy. https://agenda.infn.it/getFile.py/access?sessionId=0&resId=0&materialId=0&confId=9862.

[67] Carrier, J.-F., Archambault, L. and Beaulieu, L. Validation of Geant4, an object-oriented Monte Carlo toolkit, for simulations in medical physics. *Med. Phys.*, 31(3):484–492, 2004.

[68] Department of Physics, University of Helsinki. Alcyone Cluster documentation. http://docs.physics.helsinki.fi/alcyone.html, referred 8.5.2017.

[69] Department of Physics, University of Helsinki. Alcyone quick start: useful commands. http://docs.physics.helsinki.fi/_downloads/alcyone_mpi_quick_start.pdf, referred 11.8.2018.

[70] SchedMD. Slurm Workload Manager website. https://slurm.schedmd.com/overview.html, last modified 6.3.2013, referred 6.1.2018.

[71] White, D. R., Griffith, R. V. and Wilson, I. J. ICRU report 46: Photon, electron, proton and neutron interaction data for body tissues. *Journal of the ICRU*, 24(1), 1992.

[72] CIRS Tissue Simulation Phantom Technology. *Adult Female Phantom Model 702-D User Guide*. ATOM Dosimetry Phantoms, Document 032210.

[73] CIRS Tissue Simulation Phantom Technology. *ATOM Dosimetry Phantoms, Models 701-706*. ATOM Dosimetry Phantoms, ATOM PB 111215, 2013.

[74] Matsumoto, M. and Nishimura, T. Mersenne twister: A 623-dimensionally equidistributed uniform pseudo-random number generator. *ACM Transactions on Modeling and Computer Simulation*, 8(1):3–30, 1998.

[75] Geant4 Collaboration. Physics Reference Manual. Geant4 version 10.3, 9.12.2016.

[76] Poludniowski, G. and Evans, P. SpekCalc website. http://spekcalc.weebly.com, referred 4.7.2018.

[77] Poludniowski, G. A Quick Guide To SpekCalc. SpekCalc V 1.0 Package, http://spekcalc.weebly.com.

[78] Best Medical Canada Ltd. *Operator's Manual for the Mobile MOSFET Wireless Dosimetry System*. Document 101735.12, April 2010.

[79] Koivisto, J., Kiljunen, T., Wolf, J. and Kortesniemi, M. Characterization of MOSFET dosimeter angular dependence in three rotational axes measured free-in-air and in soft-tissue equivalent material. *Journal of Radiation Research*, 00:1–7, 2013.

[80] Siemens. *SOMATOM Definition Edge. System Owner Manual - Dosimetry and Imaging Performance Report*. Syngo CT VA48A, C2-031-1.629.03.02.02, 2014-2015.

[81] GitHub. Shaded error bars for Matlab. https://github.com/raacampbell/shadedErrorBar, version 28.9.2018, referred 17.11.2018.

[82] Attix, F. H. *Introduction to Radiological Physics and Radiation Dosimetry.* John Wiley & Sons, 1986.

[83] International Atomic Energy Agency. *Dosimetry in Diagnostic Radiology: An international Code of Practice.* Technical Reports Series No. 457, 2007.

[84] Chen, W., Kolditz, D., Beister, M., Bohle, R. and Kalender, W. A. Fast on-site Monte Carlo tool for dose calculations in CT applications. *Med. Phys.*, 39(6), 2012.